# Estimating the DOA and the Polarization of a Polynomial-Phase Signal Using a Single Polarized Vector-Sensor

Xin Yuan, *Student Member, IEEE*

***Abstract*—This paper introduces a novel algorithm to estimate the direction-of-arrival (DOA) and the polarization of a completely-polarized polynomial-phase signal of an *arbitrary* degree. The algorithm utilizes a polarized vector-sensor, comprising a spatially collocated six-component electromagnetic vector-sensor, a dipole triad, or a loop triad. This ESPRIT-based algorithm is based on a *time-invariant* matrix-pencil pair, derived from the time-delayed data-sets collected by a single polarized vector-sensor. The high-order difference-function of the signal's phase constructs the invariant-factor used in the ESPRIT algorithm. The steering vector is estimated from the signal-subspace eigenvector of the data-correlation matrix, following which the closed-form DOA and polarization can be obtained. Given the degree of the polynomial-phase signal, this approach resolves the two-dimensional azimuth-elevation angle and the polarization of the source, and requires *neither a priori* knowledge of the polynomial-phase signal's coefficients *nor a priori* knowledge of the polynomial-phase signal's frequency-spectrum. The efficacy of the proposed algorithm is verified by Monte Carlo simulations. Estimation accuracies of the DOA and the polarization parameters are evaluated by the *closed-form* Cramér–Rao bounds, which are *independent* of the polynomial coefficients, the degree of the polynomial-phase signal, and the azimuth-angle of the source.**

***Index Terms*—Antenna arrays, array signal processing, direction-of-arrival estimation, eigenvalues and eigenfunctions, FM radar, polarization, polynomial approximation, radar signal processing.**

## I. Introduction

A new ESPRIT-based algorithm is introduced in this paper to estimate the two-dimensional azimuth-elevation angle and the polarization of a completely-polarized polynomial-phase signal with a *single* collocated electromagnetic vector-sensor or a dipole/loop triad. Given the degree of the polynomial-phase signal, the proposed algorithm requires *neither a priori* knowledge of the polynomial-coefficients, *nor a priori* knowledge of the signal's frequency-spectrum. An additional contribution of this work is that the *closed-form* Cramér–Rao bounds are derived to evaluate the estimation accuracy.

Manuscript received April 27, 2011; revised August 10, 2011 and September 27, 2011; accepted November 15, 2011. Date of publication November 23, 2011; date of current version February 10, 2012. The associate editor coordinating the review of this manuscript and approving it for publication was Prof. Sofiene Affes.

The author is with the Department of Electronic and Information Engineering, Hong Kong Polytechnic University, Kowloon, Hong Kong (e-mail: eiex.yuan@connect.polyu.hk).

Color versions of one or more of the figures in this paper are available online at http://ieeexplore.ieee.org.

Digital Object Identifier 10.1109/TSP.2011.2177263

The polarized vector-sensor developed in this paper includes the following:

i) a dipole triad (a.k.a. a tripole) [3], [4], [42], [67] comprising three orthogonally-collocated *dipoles* used to measure the three components of the signal's electric field;
ii) a loop triad [42], [67] comprising three orthogonally-collocated *loops* used to measure the three components of the signal's magnetic field;
iii) a six-component electromagnetic vector-sensor [13], [19], [34], [37]–[40] comprising one dipole triad and one loop triad; these two triads are spatially collocated.

The polarized vector-sensor can resolve both the polarization and the DOA differences of the source [11], [13]. Because all antennas in the vector-sensor are *collocated*, the array-manifold of a vector-sensor is *independent* of the signal's frequency-spectrum [19]. These polarized vector-sensors have been investigated extensively for direction finding and polarization estimation: [11], [13], [15], [19], [34], [37]–[40], [47], [50], [51], [54], [58], [60], [64]–[66], [76]. Overlooked in the literature, however, is how to resolve the arriving angles and polarization of a polynomial-phase signal simultaneously. Reference [40] studied the localization for wideband sources using the electromagnetic vector-sensor, but the proposed algorithm therein was limited to the fast frequency-hop signal. Reference [47] investigated the separation and tracking of multiple broadband sources utilizing one electromagnetic vector sensor, but not for direction finding and the sources were not polynomial-phase signals. References [65] and [66] derived MUSIC-based algorithms to estimate DOA and polarization of wideband cyclostationary sources, and linear frequency modulation (LFM) signals with a single electromagnetic vector-sensor, respectively.

Based on the unique configuration of the six-component electromagnetic vector-sensor, Wong and Zoltowski propose a "uni-vector-sensor ESPRIT" algorithm [19] to resolve the DOA and the polarization diversity of multiple sources by a vector-sensor. The algorithm is also used in [77] for a spatially-spread electromagnetic vector-sensor. This algorithm investigates the *time-invariant* property of data-vectors collected by a single vector-sensor, and the matrix-pencil pair used in the ESPRIT [6] (estimation of signal parameters via rotational invariance techniques) is constituted by the two time-delayed data-vectors. However, the "uni-vector-sensor ESPRIT" algorithm in [19] and [77] is limited to sinusoidal sources (first-order polynomial-phase signals).

This paper will adopt the *time-invariant* ESPRIT to a polarized vector-sensor in a polynomial-phase source scenario. Such a situation arises, for example, in radar signal processing for source-localization and source-tracking. The polynomial-phase signal (PPS) can be of an *arbitrary* degree. A new algorithm will be pioneered to simultaneously resolve the DOA and the polarization diversity of a polynomial-phase signal by a single polarized vector-sensor. Unlike the approach used in [65] and [66], the proposed algorithm requires no iterative search and the LFM signal will be involved as a degenerate case.

### A. Summary of the Literature on the Polynomial-Phase Signal

The polynomial-phase signal has wide applications in radar, sonar and communication systems. Different signals are used in these systems with the phase as a continuous function of time. This function on a closed interval can be approximated by polynomials from the Weierstrass theorem [48]. Therefore, the phase of such a signal can be modeled as a finite-order polynomial within a limited time-interval. For example, the LFM signal [55] (also know as the chirp signal) corresponds to a second-order PPS. The quadratic frequency modulation signal is a third-order PPS in radar [1]. The received signal of radar will be a second-order PPS if a transmitted signal with constant frequency impinges a target with a constant acceleration [8].

The polynomial-phase signal has attracted considerable attention in the literature:

a) Various algorithms have been derived to estimate the amplitude, frequency and polynomial-coefficients of a polynomial-phase signal: [7], [9], [14], [16], [17], [25], [26], [29], [31], [41], [46], [53], [56], [57], [59], [61]–[63], [69], [70], [72]–[75].
b) Direction-of-arrival estimation has been studied in cases where the polynomial-phase signal impinges on a sensor array: [36], [43], [49], [55], [56], [72].
c) Theoretical bounds have been derived for the estimation of the amplitude, frequency and polynomial-coefficients of the polynomial-phase signal: [7], [8], [12], [23], [29]–[32], [41], [57].
d) High-order ambiguity function has been explored for the polynomial-phase signal in [17], [18], and [20].
e) Frequency tracking of the polynomial-phase signal has been studied in [21] and [27].
f) The modeling of the polynomial-phase signal has been explored in [33] and [45].
g) The spectral property of the polynomial-phase signal has been investigated in [24].
h) Aliasing of polynomial-phase signal parameters has been studied in [35], [52], and [71].

Previous studies utilized a sensor array to estimate the direction-of-arrival of the polynomial-phase signal. For example, [36], [43], [49], and [55] were based on the time-frequency analysis of the signal. Reference [56] proposed an extended Kalman filter-based algorithm to estimate the state of the system using a uniform linear array. Reference [72] investigated a maximum likelihood direction-finding technique based on an extended invariance property for a uniform linear array. Though the algorithm in [72] was derived in time-domain, the one-dimensional DOA was estimated by a one-dimensional search.

### B. Contributions of This Work

While both the polynomial-phase signal and the polarized vector-sensor have been investigated extensively and have various applications, it appears that to date no paper has addressed the two-dimensional DOA and polarization estimation of a polynomial-phase signal *simultaneously*. This paper aims to fill this gap by adopting the polarized vector-sensor to estimate the DOA and the polarization of a polynomial-phase signal. The proposed algorithm can offer closed-form two-dimensional DOA and polarization estimation of the signal with *no* iterative search. Furthermore, unlike [36], [43], [55], [56], and [72], the proposed algorithm is derived from the data-sets collected by a *single* polarized vector-sensor, not a sensor array. The specific contributions of this work are described below.

- The ESPRIT algorithm is adopted in a polynomial-phase source scenario with a single polarized vector-sensor.
  - Since a single polarized vector-sensor is employed, no *spatial*-invariant can be used and the conventional spatial-invariant ESPRIT is no longer applicable, therefore the time-invariant ESPRIT algorithm is utilized. As described earlier, this time-invariant ESPRIT has been investigated in [19], but the investigation was limited to the pure-tone signal. This paper will extract the time-invariant factor for an arbitrary degree PPS by the high-order difference-function of the signal's phase.
  - The high-order difference-function of the signal's phase derived from the time-delayed data-sets collected by a single polarized vector-sensor will be used as the invariant-factor in the ESPRIT algorithm.
    The second-order difference-function was used in [7] and the third-order difference-function was used in [14]. Both were used to estimate the polynomial coefficients. Similar difference-function approaches were investigated in [5], [9]. This paper will extend this difference-function to a polynomial-phase signal of an *arbitrary* degree for the polarized vector-sensor.
    Because the phase of a $q$-degree PPS is a $q$-order polynomial, the $q$th difference-function of this polynomial is a constant [2], [5], [22]. Therefore, the matrix-pencil pair used in the ESPRIT algorithm is accomplished by $(q-1)$ times recursive-computation of the $q$ time-delayed data-sets. The proposed algorithm based on this high-order difference-function is used to estimate the steering vector, and in turn the DOA and the polarization of the polynomial-phase signal.
  - The polynomial-phase signal is resolved in *time-domain*. Unlike the customary direction-finding methods for the wideband signal implemented in the frequency-domain (for example, [28]), the proposed approach resolves the direction-finding and polarization-diversity of the polynomial-phase signal in time-domain. Therefore, it requires neither Fourier transformation nor any focusing transformation.
  - The polarized vector-sensor is employed to estimate the two-dimensional DOA and the polarization of the polynomial-phase signal *simultaneously*.
  - The *closed-form* Cramér–Rao bounds of the two-dimensional DOA and the polarization parameters

of the signal are derived to evaluate the estimation accuracy. The derived Cramér–Rao bounds are *independent* of the polynomial coefficients, the degree of the polynomial-phase signal, and the azimuth-angle of the source. This is consistent with the fact that the array-manifold of the vector-sensor is independent of the frequency-spectrum of the source.

With *a priori* knowledge of the degree of the polynomial-phase signal, the proposed algorithm can offer the following advantages:

i) it can be utilized for a polynomial-phase signal of an *arbitrary* degree;
ii) it requires *no a priori* knowledge of the polynomial-phase signal's coefficients and *no a priori* knowledge of the polynomial-phase signal's frequency-spectrum;
iii) it can afford *closed-form* estimates for both the two-dimensional DOA and the polarization of the polynomial-phase signal with no iterative search.

### C. Organization of This Paper

The remainder of this paper is organized as follows: Section II provides the mathematical models of the polarized vector-sensor and the polynomial-phase signal. Section III presents the ESPRIT-based algorithm for DOA and polarization estimation of a polynomial-phase signal using one polarized vector-sensor. Section IV derives the closed-form Cramér–Rao bounds of the polarized vector-sensor in one polynomial-phase source scenario. Section V presents the simulation results of the proposed algorithm. Section VI concludes the whole paper.

## II. Mathematical Models of the Polynomial-Phase Signal and the Polarized Vector-Sensor

### A. Mathematical Model of the Polynomial-Phase Signal

The polynomial-phase signal can be modeled in continuous time as

$$s(t;\boldsymbol{\psi}) = \sqrt{\mathcal{P}}\exp\{j\boldsymbol{\varphi}(t;\boldsymbol{\psi})\} \tag{1}$$

$$\boldsymbol{\varphi}(t;\boldsymbol{\psi}) = b_0 + b_1 t + b_2 t^2 + \cdots + b_q t^q \tag{2}$$

where $\boldsymbol{\psi} = (b_0, b_1, \ldots, b_q)^T$ is a vector that contains the parameters in the polynomial phase $\boldsymbol{\varphi}(t;\boldsymbol{\psi})$, with $b_\ell$ $(\ell = 0, 1, 2, \ldots, q)$ symbolizing the $\ell$-order coefficient, $^T$ denotes transposition, and $q$ is the degree of the polynomial-phase signal. The initial phase of the polynomial-phase signal is $b_0$, and the power is $\mathcal{P}$.

### B. Mathematical Model of the Polarized Vector-Sensor

The three dipoles composing the dipole triad can measure the three components of the electric field of the signal. With the definition of azimuth-elevation angle $(\theta_1, \theta_2)$ illustrated in Fig. 1, the response of a dipole triad can be expressed as [3], [4], [11], [42]

$$\mathbf{e} \overset{\text{def}}{=} \begin{bmatrix} e_x \\ e_y \\ e_z \end{bmatrix} \overset{\text{def}}{=} \begin{bmatrix} \cos\theta_1 \sin\theta_2 \sin\theta_3 e^{j\theta_4} - \sin\theta_1 \cos\theta_3 \\ \sin\theta_1 \sin\theta_2 \sin\theta_3 e^{j\theta_4} + \cos\theta_1 \cos\theta_3 \\ -\cos\theta_2 \sin\theta_3 e^{j\theta_4} \end{bmatrix}$$

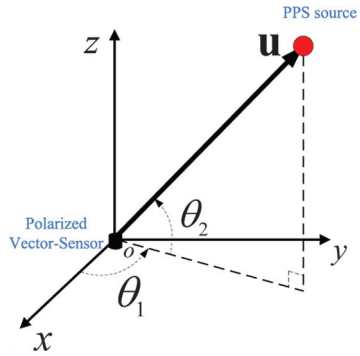


Fig. 1. Geometry of polarized vector-sensor and polynomial-phase signal. $\theta_1 \in [0, 2\pi)$ denotes the azimuth angle and $\theta_2 \in \left[\frac{-\pi}{2}, \frac{\pi}{2}\right]$ symbolizes the elevation angle of the polynomial-phase source.

where $(\theta_3, \theta_4)$ denote the auxiliary polarization angle and polarization phase difference, respectively (equating to $(\gamma, \eta)$ in [11]). In this paper, only the completely-polarized signal is investigated, thus $(\theta_3, \theta_4)$ are modeled as time-invariant. The anti-jamming performance of the dipole triad was investigated by Compton in [3], and [4] and Wong studied the direction finding and polarization estimation by a single dipole triad in [42]. Li adopted a loop triad together with a dipole triad to estimate the DOA and polarization of the source in [11] and Nehorai and Paldi investigated the relationship between the electric field and magnetic field in [13]. The three components of the magnetic field measured by the loop triad can be expressed as [13]

$$\mathbf{h} \overset{\text{def}}{=} \mathbf{u} \times \mathbf{e} \overset{\text{def}}{=} [h_x, h_y, h_z]^T \overset{\text{def}}{=} \begin{bmatrix} -\sin\theta_1 \sin\theta_3 e^{j\theta_4} - \cos\theta_1 \sin\theta_2 \cos\theta_3 \\ \cos\theta_1 \sin\theta_3 e^{j\theta_4} - \sin\theta_1 \sin\theta_2 \cos\theta_3 \\ \cos\theta_2 \cos\theta_3 \end{bmatrix}$$

where $\times$ symbolizes vector cross-product operator and $\mathbf{u} = [\cos\theta_2 \cos\theta_1, \cos\theta_2 \sin\theta_1, \sin\theta_2]^T$ shown in Fig. 1. Nehorai & Paldi studied the electromagnetic vector-sensor by collocating the dipole triad and loop triad at one point geometry [13]. Thus, the six-component electromagnetic vector-sensor can measure both the electric field and magnetic field simultaneously. The array-manifold can be expressed mathematically as

$$\mathbf{a} \overset{\text{def}}{=} [\mathbf{e}^T, \mathbf{h}^T]^T = [e_x, e_y, e_z, h_x, h_y, h_z]^T. \tag{3}$$

In order to simplify the exposition, all parameters to be estimated in the following section are collected in $\boldsymbol{\theta} = [\theta_1, \theta_2, \theta_3, \theta_4]^T$.

## III. Proposed Algorithm

### A. Basic Principle Underlying the New Algorithm

ESPRIT requires two identical but translated subvectors to implement the rotational invariance technique. These subvectors can be constructed by two subarrays [6] or two time-delayed data-sets [19]. The basic principle of the proposed algorithm is to construct the two subvectors using the data-sets collected by a *single* polarized vector-sensor.

Recall that the phase of a PPS in (2), $\boldsymbol{\varphi}(t;\boldsymbol{\psi})$ is a $q$-order polynomial of $t$. From the relevant mathematical knowledge [2] and [5], [9], the $q$-order *difference-function* of $\boldsymbol{\varphi}(t;\boldsymbol{\psi})$ is a constant

and is thus *time-independent*. This $q$-order difference-function of $\boldsymbol{\varphi}(t;\boldsymbol{\psi})$ can be accomplished by a recursive-computation of the $(q+1)$ time-delayed data-sets collected by a single polarized vector-sensor. Following the above recursive manipulation, two data-vectors will be obtained within a rotational invariant-factor and hence the ESPRIT can be adopted straightforwardly. The following will show why and how.

### B. The Measurement Model

Suppose there is a far-field source emitting a polynomial-phase signal. The data-set measured by a six-component electromagnetic vector-sensor is

$$\mathbf{x}(t) = \mathbf{a}(\boldsymbol{\theta})s(t) + \boldsymbol{\varepsilon}(t) \tag{4}$$

where $\mathbf{a}(\theta)$ is the array-manifold of the six-component electromagnetic vector-sensor as in (3) and $s(t)$ is the PPS as in (1). In this work, $\boldsymbol{\varepsilon}(t)$ is modeled as zero mean, complex Gaussian distributed, and with a variance of $6\times 6$ diagonal matrix $\mathrm{diag}[\sigma^2,\sigma^2,\sigma^2,\sigma^2,\sigma^2,\sigma^2]$, where $\sigma^2$ denotes the variance of noise collected by each constituent antenna.

### C. Deriving the Matrix-Pencil Pair

For a six-component electromagnetic vector-sensor, from (4):

$$\begin{aligned}\mathbf{x}(t) &= \mathbf{a}s(t) + \boldsymbol{\varepsilon}(t)\\ &= [e_x, e_y, e_z, h_x, h_y, h_z]^T\, s(t) + \boldsymbol{\varepsilon}(t).\end{aligned}$$

In order to simplify the exposition, we consider the *noiseless* case in the following derivation. Consider a $q$-order polynomial phase signal, and let $\mathbf{x}_{(q)}(t)$ be the vector-sensor measured data for this signal. In the *noiseless* case:

$$\mathbf{x}_{(q)}(t) = [e_x, e_y, e_z, h_x, h_y, h_z]^T\, s(t).$$

The $\mathbf{x}_{(q)}(t)$ is a $6\times 1$ vector and let $x_{i,q}(t)$ be the $i$th row of $\mathbf{x}_{(q)}(t)$, $\forall i = 1,2,\ldots,6$. With $T_s$ to denote the sampling time-interval, consider there are $M$ time samples, $\left[\mathbf{x}_{(q)}(T_s), \mathbf{x}_{(q)}(2T_s), \ldots, \mathbf{x}_{(q)}(MT_s)\right]$.

When $q \geq 2$, carry on the computation in the following box, $\forall m = 1,2,\ldots,(M-q+1)$:

1) It is inferred that for any $\delta_T \neq 0$, $\mathbf{x}_{(q-1)}(mT_s)$ is computed by $\mathbf{x}_{(q)}(mT_s)x^*_{i,q}(mT_s+\delta_T)$, where $^*$ denotes the complex conjugation. This means:

$$\mathbf{x}_{(q-1)}(mT_s) = \mathbf{x}_{(q)}(mT_s)x^*_{i,q}(mT_s+\delta_T), \quad \forall m = 1,2,\ldots,(M-q+1). \tag{5}$$

2) Repeat step 1) for $q = q-1$ until $\mathbf{x}_{(1)}(mT_s)$ is reached. For the $q$-order PPS, in total there are $(q-1)$ times recursive computation for step 1).

In the box above, $\delta_T$ is a constant time-delay, and in the practical application, $\delta_T$ can be selected as $\delta_T = pT_s$.

It is known that for every recursive computation of step 1), the one-order difference-function of the signal's phase is derived [2]. Since the $\boldsymbol{\varphi}(t;\boldsymbol{\psi})$ is a $q$-order polynomial of $t$, the $(q-1)$-order difference-function is a first-order polynomial. Thus, $\mathbf{x}_{(1)}(t), t = mT_s$ is a first-order polynomial of $t$. With some manipulation:

$$\begin{aligned}\mathbf{x}_{(1)}(mT_s) &= \mathbf{a}\left(|[\mathbf{a}]_i|^{\left(2^{(q-2)}-1\right)}[\mathbf{a}]_i^*\right)\\ &\quad\cdot e^{j(-1)^{(q-1)}\left[f(\delta_T,b_{q-1},b_q)+(q!)b_q\delta_T^{(q-1)}mT_s\right]}\\ &= \underbrace{\mathbf{a}\left(|[\mathbf{a}]_i|^{\left(2^{(q-2)}-1\right)}[\mathbf{a}]_i^*\right)\cdot e^{j(-1)^{(q-1)}f(\delta_T,b_{q-1},b_q)}}_{\stackrel{\mathrm{def}}{=}\tilde{\mathbf{a}}}\\ &\quad\cdot e^{j(-1)^{(q-1)}(q!)b_q\delta_T^{(q-1)}mT_s},\ \forall q\geq 2\end{aligned} \tag{6}$$

where $[\mathbf{a}]_i$ denotes the $i$th element in $\mathbf{a}$, $|[\mathbf{a}]_i|$ is the absolute value of $[\mathbf{a}]_i$, $q! = 1\times 2\times 3\times\cdots\times q$ refers to the factorial of $q$, and $f(\delta_T, b_{q-1}, b_q)$ is a function of the parameters in the $()$. Note that $f(\delta_T, b_{q-1}, b_q)$ is independent of $t$ and for different $q$, it has different values.

Introducing another constant time-delay $\Delta_T$:

$$\begin{aligned}\mathbf{x}_{(1)}(mT_s) &= \tilde{\mathbf{a}}e^{j(-1)^{(q-1)}(q!)b_q\delta_T^{(q-1)}mT_s},\\ \mathbf{x}_{(1)}(mT_s+\Delta_T) &= \tilde{\mathbf{a}}e^{j(-1)^{(q-1)}(q!)b_q\delta_T^{(q-1)}(mT_s+\Delta_T)}\\ &= \mathbf{x}_{(1)}(mT_s)e^{j(-1)^{(q-1)}(q!)b_q\delta_T^{(q-1)}\Delta_T}.\end{aligned}$$

In the practical application, $\Delta_T$ can be selected as $\Delta_T = \ell T_s$, where $\ell$ is a positive integer. $\Delta_T$ can be the same as or different from $\delta_T$.

The $12\times 1$ data-set can then be shown as

$$\begin{aligned}\mathbf{y}(mT_s) &\stackrel{\mathrm{def}}{=} \begin{bmatrix}\mathbf{x}_{(1)}(mT_s)\\ \mathbf{x}_{(1)}(mT_s+\Delta_T)\end{bmatrix} \stackrel{\mathrm{def}}{=} \begin{bmatrix}\mathbf{y}_1(mT_s)\\ \mathbf{y}_2(mT_s)\end{bmatrix}\\ &= \begin{bmatrix}\mathbf{y}_1(mT_s)\\ \mathbf{y}_1(mT_s)e^{j(-1)^{(q-1)}b_q(q!)\delta_T^{(q-1)}\Delta_T}\end{bmatrix}.\end{aligned}$$

Note that $e^{j(-1)^{(q-1)}b_q(q!)\delta_T^{(q-1)}\Delta_T}$ depends on i) the highest-order polynomial-coefficient $b_q$, ii) the degree of the polynomial-phase signal $q$, and iii) the time-delays $\{\delta_T, \Delta_T\}$, all of which are *constants*. Thus, $e^{j(-1)^{(q-1)}b_q(q!)\delta_T^{(q-1)}\Delta_T}$ is *time-independent* and will be used as the *invariant-factor* in the following ESPRIT algorithm.

Suppose there are $N$ snapshots, $(N \leq (M-q+1))$, collected in $\{\mathbf{x}_{(1)}(mT_s), \mathbf{x}_{(1)}(mT_s+\Delta_T)\}$. Then, form the $12\times N$ data-set

$$\mathbf{Y} \stackrel{\mathrm{def}}{=} [\mathbf{y}(T_s), \mathbf{y}(2T_s), \ldots, \mathbf{y}(NT_s)] \stackrel{\mathrm{def}}{=} \begin{bmatrix}\mathbf{Y}_1\\ \mathbf{Y}_2\end{bmatrix}. \tag{7}$$

*Remarks:*

- In (5), step 1) to compute the $\mathbf{x}_{(1)}(mT_s)$, any one row in $\mathbf{x}_{(q)}(mT_s)$ can be used. This does not affect the following derivation. In cases when any one row is equal to zero, we can use any other nonzero entity.
- Equation (5) in step 1) can be changed to

$$\mathbf{x}_{(q-1)}(mT_s) = \sum_{i=1}^{6}\mathbf{x}_{(q)}(mT_s)x^*_{i,q}(mT_s+\delta_T). \tag{8}$$

  Although (8) will increase the computation workload, it has the following advantages: a) preserving the signal, b) enhancing the noise cancelation, and c) avoiding the case when one row in $\mathbf{x}_{(q)}(t)$ is equal to zero.
- If the dipole/loop triad is used, (8) will become

$$\mathbf{x}_{(q-1)}(mT_s) = \sum_{i=1}^{3}\mathbf{x}_{(q)}(mT_s)x^*_{i,q}(mT_s+\delta_T).$$

- Equation (6) holds in the single-source scenario and also for the algorithm derived in this section. In the multiple-source scenario, the algorithm to separate and enhance the source-of-interest (for example, [47]) should first be used and then the proposed algorithm can be adopted in a single-source scenario.
- In the *noisy* case, *multiplicative noise* will be introduced in (5). Equation (6) will become approximated. When the noise power $\sigma^2$ increases, the noise will affect the algorithm adversely. With the fixed PPS at the deterministic DOA and polarization parameters, when the degree of the PPS increases, the repetitions of step 1) will increase. Thus, more *multiplicative noise* will be introduced, which will affect the algorithm more seriously. The simulation results at low signal-to-noise ratio (SNR) in Section V verify this point.

### D. Adopting ESPRIT to the Data-Set $\mathbf{Y}$

The data-set $\mathbf{Y}$ in (7) can be seen as a data-vector based on the vector $\tilde{\mathbf{a}}$ defined in (6) (which is modified from the array-manifold $\mathbf{a}$). Compute the correlation matrix of the $12 \times N$ data measurements:

$$\mathbf{Y}\mathbf{Y}^H = \begin{bmatrix} \mathbf{Y}_1 \\ \mathbf{Y}_2 \end{bmatrix} [\, \mathbf{Y}_1^H \quad \mathbf{Y}_2^H \,] = \begin{bmatrix} \mathbf{Y}_1\mathbf{Y}_1^H & \mathbf{Y}_1\mathbf{Y}_2^H \\ \mathbf{Y}_2\mathbf{Y}_1^H & \mathbf{Y}_2\mathbf{Y}_2^H \end{bmatrix},$$

and then carry on the eigen-decomposition, where $^H$ denotes conjugate transposition.

Similar to [19, Sec. III-B], there are two estimates of the steering vector $\hat{\mathbf{v}}_1$ (corresponding to $\mathbf{Y}_1\mathbf{Y}_1^H$), $\hat{\mathbf{v}}_2$ (corresponding to $\mathbf{Y}_2\mathbf{Y}_2^H$). Since in the present work, we only consider the one-source scenario, these two estimates are obtained from the eigenvector of $\mathbf{Y}\mathbf{Y}^H$ associated with the largest eigenvalue ($\hat{\mathbf{v}}_1$ corresponds to the top $6 \times 1$ subvector and $\hat{\mathbf{v}}_2$ corresponds to the bottom $6 \times 1$ subvector). They are inter-related by the value $\rho = e^{j(-1)^{(q-1)}(q!)b_q\delta_T^{(q-1)}\Delta_T}$ and this $\rho$ can be estimated by the two estimated steering vectors $\hat{\mathbf{v}}_1$, $\hat{\mathbf{v}}_2$ through

$$\hat{\rho} = (\hat{\mathbf{v}}_1^H\hat{\mathbf{v}}_1)^{-1}\hat{\mathbf{v}}_1^H\hat{\mathbf{v}}_2. \tag{9}$$

Therefore, $\tilde{\mathbf{a}}$ can be estimated from $\hat{\mathbf{v}}_1$, $\hat{\mathbf{v}}_2$ by (within an unknown complex number $c$)[1]:

$$\hat{\tilde{\mathbf{a}}} = \frac{1}{2}\left(\hat{\mathbf{v}}_1 + \frac{\hat{\mathbf{v}}_2}{\hat{\rho}}\right) = c\tilde{\mathbf{a}}. \tag{10}$$

It is worth noting that the algorithm can be used for an *arbitrary* degree polynomial-phase signal[2] (i.e., if $q = 2$, it is an LFM signal). Given the degree of the polynomial-phase signal, the algorithm requires *no a priori* knowledge of the polynomial coefficients. Since the derivation of the matrix-pencil pair depends solely on the degree of the PPS, the efficacy of the proposed algorithm is *independent* of the polynomial coefficients of the signal.

### E. Closed-Form Formulas to Estimate Azimuth-Elevation Angle and Polarization Parameters

From the estimate in (10), one can obtain the estimate of $\hat{\tilde{\mathbf{a}}}$, within an *unknown* complex number $c$. From this $\hat{\tilde{\mathbf{a}}}$, the DOA and polarization of the PPS can be estimated. The following derives the closed-form formulas.

*1) Closed-Form Estimation Formulas for the Six-Component Electromagnetic Vector-Sensor:*

$$\hat{\tilde{\mathbf{a}}} = c\tilde{\mathbf{a}} \stackrel{\text{def}}{=} c\left[\acute{\mathbf{e}}^T, \acute{\mathbf{h}}^T\right]^T$$

where $\acute{\mathbf{e}} = [[\tilde{\mathbf{a}}]_1, [\tilde{\mathbf{a}}]_2, [\tilde{\mathbf{a}}]_3]^T$ and $\acute{\mathbf{h}} = [[\tilde{\mathbf{a}}]_4, [\tilde{\mathbf{a}}]_5, [\tilde{\mathbf{a}}]_6]^T$, with $[\tilde{\mathbf{a}}]_i$ denoting the $i$th element in $\tilde{\mathbf{a}}$, $\forall i = 1, 2, \ldots, 6$. From the vector-cross-product, $\hat{\mathbf{u}} = \frac{c\acute{\mathbf{e}} \times (c\acute{\mathbf{h}})^*}{\|c\acute{\mathbf{e}} \times (c\acute{\mathbf{h}})^*\|}$, where $\|\cdot\|$ denotes the Frobenius norm of the element inside $\|\cdot\|$, $\times$ is the vector-cross-product operation, and $^*$ symbolizes complex conjugation. This relation is similar to the equations used in [19], [34], and [37]–[40], [42] and is critical to the estimation of direction-cosines for the six-component electromagnetic vector-sensor.

The DOA can be estimated by [19]

$$\hat{\theta}_1 = \angle\left([\hat{\mathbf{u}}]_1 + j[\hat{\mathbf{u}}]_2\right), \quad \hat{\theta}_2 = \arcsin\left([\hat{\mathbf{u}}]_3\right)$$

where $\angle(\cdot)$ denotes the angle of complex number in $(\cdot)$.

The polarization parameters can be estimated by

$$\hat{\theta}_3 = \arctan\left|\frac{[\hat{\tilde{\mathbf{a}}}]_3}{[\hat{\tilde{\mathbf{a}}}]_6}\right|, \quad \hat{\theta}_4 = \angle\left(\frac{[\hat{\tilde{\mathbf{a}}}]_3}{[\hat{\tilde{\mathbf{a}}}]_6}\right) - \pi.$$

*2) Closed-Form Estimation Formulas for the Dipole/Loop Triad:*

a) For the dipole triad, $\hat{\tilde{\mathbf{e}}} = c\tilde{\mathbf{e}} = c\,[[\tilde{\mathbf{a}}]_1, [\tilde{\mathbf{a}}]_2, [\tilde{\mathbf{a}}]_3]^T$:

$$\begin{aligned}\mathbf{d} &\stackrel{\text{def}}{=} \left[\frac{[\hat{\tilde{\mathbf{e}}}]_1}{[\hat{\tilde{\mathbf{e}}}]_3}, \frac{[\hat{\tilde{\mathbf{e}}}]_2}{[\hat{\tilde{\mathbf{e}}}]_3}\right]^T = \left[\frac{e_x}{e_z}, \frac{e_y}{e_z}\right]^T \\ &= \begin{bmatrix} -\cos\theta_1\tan\theta_2 + \frac{\sin\theta_1}{\cos\theta_2}\cot\theta_3\cos\theta_4 \\ -\sin\theta_1\tan\theta_2 - \frac{\cos\theta_1}{\cos\theta_2}\cot\theta_3\cos\theta_4 \end{bmatrix} \\ &\quad + j\begin{bmatrix} -\frac{\sin\theta_1}{\cos\theta_2}\cot\theta_3\sin\theta_4 \\ \frac{\cos\theta_1}{\cos\theta_2}\cot\theta_3\sin\theta_4 \end{bmatrix}.\end{aligned}$$

b) For the loop triad, $\hat{\tilde{\mathbf{h}}} = c\tilde{\mathbf{h}} = c\,[[\tilde{\mathbf{a}}]_4, [\tilde{\mathbf{a}}]_5, [\tilde{\mathbf{a}}]_6]^T$:

$$\begin{aligned}\mathbf{d} &\stackrel{\text{def}}{=} \left[\frac{[\hat{\tilde{\mathbf{h}}}]_1}{[\hat{\tilde{\mathbf{h}}}]_3}, \frac{[\hat{\tilde{\mathbf{h}}}]_2}{[\hat{\tilde{\mathbf{h}}}]_3}\right]^T = \left[\frac{h_x}{h_z}, \frac{h_y}{h_z}\right]^T \\ &= \begin{bmatrix} -\frac{\sin\theta_1}{\cos\theta_2}\tan\theta_3\cos\theta_4 - \cos\theta_1\tan\theta_2 \\ \frac{\cos\theta_1}{\cos\theta_2}\tan\theta_3\cos\theta_4 - \sin\theta_1\tan\theta_2 \end{bmatrix} \\ &\quad + j\begin{bmatrix} -\frac{\sin\theta_1}{\cos\theta_2}\tan\theta_3\sin\theta_4 \\ \frac{\cos\theta_1}{\cos\theta_2}\tan\theta_3\sin\theta_4 \end{bmatrix}.\end{aligned}$$

With the relevant mathematical manipulations:

$$\hat{\theta}_1 = \begin{cases} \tan^{-1}\left(\frac{-\Im m\{[\mathbf{d}]_1\}}{\Im m\{[\mathbf{d}]_2\}}\right), & \text{if } (\Im m\{[\mathbf{d}]_2\}\sin\theta_4) \geq 0 \\ \tan^{-1}\left(\frac{-\Im m\{[\mathbf{d}]_1\}}{\Im m\{[\mathbf{d}]_2\}}\right) + \pi, & \text{if } (\Im m\{[\mathbf{d}]_2\}\sin\theta_4) < 0 \end{cases} \tag{11}$$

[1]From (9), the $q$th-order polynomial coefficient can be estimated by: $\hat{b}_q = \frac{\angle\hat{\rho} + 2\pi m_b}{(-1)^{(q-1)}(q!)\delta_T^{(q-1)}\Delta_T}$, where $m_b$ is an integer and can be determined by *a priori* knowledge of the region of $b_q$. After the estimation of DOA and polarization, the other polynomial coefficients can be estimated from the algorithms derived in the references cited in Section I-A.

[2]If the frequency of the PPS is a constant, the PPS is first-order and so is a pure-tone. In this case, the proposed algorithm will degenerate to the "uni-vector-sensor ESPRIT" algorithm in [19]. It will require no *recursive* computation of steps 1) and 2) in Section III-C and can be used in the multiple-source scenario directly. For details, please refer to [19].

$$\hat{\theta}_2 = \begin{cases} \tan^{-1}\left(-\Re e\{[\mathbf{d}]_1\}\cos\hat{\theta}_1 - \Re e\{[\mathbf{d}]_2\}\sin\hat{\theta}_1\right), \\ \quad \text{if } \left(\Re e\{[\mathbf{d}]_1\}\cos\hat{\theta}_1 + \Re e\{[\mathbf{d}]_2\}\sin\hat{\theta}_1\right) \le 0 \\ \tan^{-1}\left(-\Re e\{[\mathbf{d}]_1\}\cos\hat{\theta}_1 - \Re e\{[\mathbf{d}]_2\}\sin\hat{\theta}_1\right) + \pi, \\ \quad \text{if } \left(\Re e\{[\mathbf{d}]_1\}\cos\hat{\theta}_1 + \Re e\{[\mathbf{d}]_2\}\sin\hat{\theta}_1\right) > 0 \end{cases}$$

$$\hat{\theta}_4 = -\angle\left([\mathbf{d}]_1\sin\hat{\theta}_1 - [\mathbf{d}]_2\cos\hat{\theta}_1\right)$$

$$\hat{\theta}_3 = \begin{cases} \cot^{-1}\left(\frac{\Im m\{[\mathbf{d}]_2\}\cos\hat{\theta}_2}{\sin\hat{\theta}_4\cos\hat{\theta}_1}\right), & \text{for the dipole triad} \\ \tan^{-1}\left(\frac{\Im m\{[\mathbf{d}]_2\}\cos\hat{\theta}_2}{\sin\hat{\theta}_4\cos\hat{\theta}_1}\right), & \text{for the loop triad} \end{cases}$$

where $\Re e\{\}$ and $\Im m\{\}$ denote the real part and the imaginary part of the entry in $\{\}$, respectively.

It is notable that the closed-form formulas for the dipole triad and the loop triad are different from the formulas in [42]. The validity region of these triads is $[\{\theta_1 \in [0, 2\pi)\} \cap \{\theta_2 \in \left[\frac{-\pi}{2}, \frac{\pi}{2}\right]\} \cap \{\theta_3 \in \left[0, \frac{\pi}{2}\right]\} \cap \{\theta_4 \in (-\pi, 0]\}]$ or $[\{\theta_1 \in [0, 2\pi)\} \cap \{\theta_2 \in [\frac{-\pi}{2}, \frac{\pi}{2}]\} \cap \{\theta_3 \in [0, \frac{\pi}{2}]\} \cap \{\theta_4 \in (0, \pi]\}]$. This is because the sign of $\sin\theta_4$ needs to be *a priori* knowledge when (11) is used to estimate the azimuth-angle $\theta_1$. In contrast, the validity region of the six-component electromagnetic vector-sensor is the entire sphere, and requires no *a priori* knowledge.

## IV. Cramér–Rao Bounds Derivation

The Cramér–Rao bounds of direction-of-arrival and polarization for the six-component electromagnetic vector-sensor were derived in [13] by modeling the signal as a zero-mean complex Gaussian-distributed random sequence. [67] derived the Cramér–Rao bounds of direction-of-arrival and polarization for the six-component electromagnetic vector-sensor, the dipole triad and the loop triad by modeling the sources as multiple pure-tones. The Cramér–Rao bounds of the polynomial coefficients, amplitude or frequency for polynomial-phase signal were derived in [8], [12], [23], [29], [32], [56], [57], [61] and used in [16], [17], [26], [27], [31], [41], [52], [53], [59], [62], [63], [68], [70], [73]–[75]. [43], and [72] derived the Cramér–Rao bounds of DOA with the polynomial-phase signal for the isotropic sensor array.

Unlike the Cramér–Rao bounds derived or used in [13], [37], [38], [42], [50], and [67] and the aforementioned studies, this paper will derive *new* Cramér–Rao bounds of the DOA and the polarization for the six-component electromagnetic vector-sensor, the dipole triad and the loop triad with one polynomial-phase signal. The derived Cramér–Rao bounds are *closed-form* expressions, explicitly in terms of the signal parameters. As in the previous studies, the additive complex Gaussian-distributed noise model will also be used in the following derivation.

### A. The Statistical Data Model

In the following derivation, the $(q+5)$ deterministic but unknown parameters are $\boldsymbol{\kappa} = [\boldsymbol{\theta}, b_0, b_1, \ldots, b_q]^T$. The noise covariance $\sigma^2$ is modeled as *a priori* known. Recall the measurement model in (4). After uniform sampling, consider in total $M$ snapshots are collected. With $T_s$ to symbolize the sampling time-interval, the collected $6 \times M$ data-vector is

$$\mathbf{X} = [\mathbf{x}(T_s), \mathbf{x}(2T_s), \ldots, \mathbf{x}(MT_s)]. \tag{12}$$

Rewrite it in a $6M \times 1$ sequence:

$$\mathbf{w} \stackrel{\text{def}}{=} \left[\mathbf{x}^T(T_s), \mathbf{x}^T(2T_s), \ldots, \mathbf{x}^T(MT_s)\right]^T \stackrel{\text{def}}{=} \mathbf{m}(\boldsymbol{\kappa}) + \mathbf{n}$$

where $\mathbf{m}(\boldsymbol{\kappa}) \stackrel{\text{def}}{=} \mathbf{a}(\boldsymbol{\theta}) \otimes \mathbf{s}$ with $\mathbf{s} \stackrel{\text{def}}{=} [s(T_s), s(2T_s), \ldots, s(MT_s)]^T$, $\mathbf{n} \sim \mathcal{N}(0, \sigma^2\mathbf{I}_{6M})$ denotes a zero-mean, Gaussian distributed process, with a covariance matrix $\mathbf{K} = \sigma^2\mathbf{I}_{6M}$, $\mathbf{I}_{6M}$ is a $6M \times 6M$ identity matrix, and $\otimes$ symbolizes the Kronecker product. It follows that $\mathbf{w} \sim \mathcal{N}(\mathbf{m}(\boldsymbol{\kappa}), \mathbf{K})$. If the three-component dipole triad or loop triad is adapted as described, the data-set $\mathbf{w}$ will be $3M \times 1$.

### B. Deriving the Cramér–Rao Bounds of the DOA and the Polarization Parameters

In the statistical data model of Section IV-A, the $(q+5)$ unknown parameters in $\boldsymbol{\kappa}$ introduces a $(q+5) \times (q+5)$ Fisher information matrix (FIM):

$$\mathbf{J} = \begin{bmatrix} J_{\theta_1,\theta_1} & J_{\theta_1,\theta_2} & J_{\theta_1,\theta_3} & J_{\theta_1,\theta_4} & J_{\theta_1,b_0} & \cdots & J_{\theta_1,b_q} \\ J_{\theta_2,\theta_1} & J_{\theta_2,\theta_2} & J_{\theta_2,\theta_3} & J_{\theta_2,\theta_4} & J_{\theta_2,b_0} & \cdots & J_{\theta_2,b_q} \\ J_{\theta_3,\theta_1} & J_{\theta_3,\theta_2} & J_{\theta_3,\theta_3} & J_{\theta_3,\theta_4} & J_{\theta_3,b_0} & \cdots & J_{\theta_3,b_q} \\ J_{\theta_4,\theta_1} & J_{\theta_4,\theta_2} & J_{\theta_4,\theta_3} & J_{\theta_4,\theta_4} & J_{\theta_4,b_0} & \cdots & J_{\theta_4,b_q} \\ J_{b_0,\theta_1} & J_{b_0,\theta_2} & J_{b_0,\theta_3} & J_{b_0,\theta_4} & J_{b_0,b_0} & \cdots & J_{b_0,b_q} \\ J_{b_1,\theta_1} & J_{b_1,\theta_2} & J_{b_1,\theta_3} & J_{b_1,\theta_4} & J_{b_1,b_0} & \cdots & J_{b_1,b_q} \\ \vdots & \vdots & \vdots & \vdots & \vdots & \ddots & \vdots \\ J_{b_q,\theta_1} & J_{b_q,\theta_2} & J_{b_q,\theta_3} & J_{b_q,\theta_4} & J_{b_q,b_0} & \cdots & J_{b_q,b_q} \end{bmatrix}. \tag{13}$$

As all the parameters are independent of $\mathbf{K}$, from (8.34) in [44] by setting the second term to zero, the $(i,j)$th entry of $\mathbf{J}$ is

$$[\mathbf{J}]_{i,j} = 2\Re e\left\{\frac{\partial\mathbf{m}^H(\boldsymbol{\kappa})}{\partial[\boldsymbol{\kappa}]_i}\mathbf{K}^{-1}\frac{\partial\mathbf{m}(\boldsymbol{\kappa})}{\partial[\boldsymbol{\kappa}]_j}\right\}. \tag{14}$$

The Cramér–Rao bounds (CRB) of direction-of-arrival and polarization estimation can be computed by

$$\text{CRB}(\theta_i) = \left[\mathbf{J}^{-1}\right]_{i,i}, \quad \forall i = 1, 2, 3, 4.$$

The closed-form Cramér–Rao bounds results for $q \le 10$,[3] can be obtained as (15)–(26) at the bottom of the next page (refer to the Appendix for derivation details).

### C. Qualitative Observations

Some qualitative observations are obtained from the closed-form Cramér–Rao bounds in Section IV-B.

1) All the closed-form Cramér–Rao bounds for the six-component electromagnetic vector-sensor, the dipole triad, and the loop triad are *independent* of i) the polynomial coefficients $\boldsymbol{\psi} = (b_0, b_1, \ldots, b_q)^T$, ii) the degree of the polynomial phase signal $q$,[4] iii) the azimuth-angle of the signal $\theta_1$, and iv) the time sample interval $T_s$.
   This may seem initially surprising but is in fact reasonable. The reasons are as follows.
   a) The array-manifold of the polarized vector-sensor is *independent* of the signal's frequency-spectrum. Even

[3]For the commonly used polynomial-phase signal, $q \le 10$ always holds.

[4]The algorithm proposed in Section III is based on the recursive computation of the auto-correlation, and it thus depends on the signal order. However, the Cramér-Rao bounds are independent of the algorithm, and so they are independent of the signal order $q$.

the high-order PPS has a broadband frequency-spectrum; it has the same Cramér–Rao bounds as the pure tone. This result is also consistent with that reported in [67], which derived the closed-form Cramér–Rao bounds of the polarized vector-sensor with sinusoidal sources. The Cramér–Rao bounds in [67] are also independent of the signal-frequency and initial phase, but they do depend on the frequency difference of the different signals.

b) All the phases of the PPS are *eliminated* when one uses (14) to compute the elements in the FIM (refer to the Appendix for all the elements of the FIM for the six-component electromagnetic vector-sensor and the dipole/loop triad).

2) The closed-form Cramér–Rao lower bound of the elevation-angle for the six-component electromagnetic vector-sensor $\mathrm{CRB}^{(em)}(\theta_2)$ is also independent of the elevation angle $\theta_2$ and the polarization parameters $(\theta_3, \theta_4)$.

3) When $\theta_3 = 0$, i) $\mathrm{CRB}^{(e)}(\theta_2)$ will be infinite and ii) $\mathrm{CRB}^{(em)}(\theta_1), \mathrm{CRB}^{(e)}(\theta_1), \mathrm{CRB}^{(h)}(\theta_1)$ will be zero.

4) When $\theta_3 = \frac{\pi}{2}$, i) $\mathrm{CRB}^{(h)}(\theta_2)$ will be infinite and ii) $\mathrm{CRB}^{(em)}(\theta_1), \mathrm{CRB}^{(e)}(\theta_1), \mathrm{CRB}^{(e)}(\theta_1), \mathrm{CRB}^{(h)}(\theta_1)$ will be zero.

5) When $\theta_4 = 0, \pi$, $\mathrm{CRB}^{(e)}(\theta_2)$, $\mathrm{CRB}^{(e)}(\theta_1)$, $\mathrm{CRB}^{(e)}(\theta_3)$, $\mathrm{CRB}^{(h)}(\theta_2)$, $\mathrm{CRB}^{(h)}(\theta_1)$, $\mathrm{CRB}^{(h)}(\theta_3)$ will be infinite.

## V. Monte Carlo Simulation

The efficacy of the proposed algorithm is demonstrated by Monte Carlo simulations. 200 independent Monte Carlo trials and 100 temporal snapshots are used in these simulations. A second-order unity-power polynomial-phase signal (also known as an LFM or a chirp signal) is used with $\{b_0 = 0.05, b_1 = 0.1, b_2 = 0.13\}$ impinging on a polarized vector-sensor. The DOA and polarization of the source are $\{\theta_1, \theta_2, \theta_3, \theta_4\} = \{53^\circ, 42^\circ, 45^\circ, 90^\circ\}$. Fig. 3 plots the

---

1) Closed-Form CRB for the Six-Component Electromagnetic Vector-Sensor:

$$\mathrm{CRB}^{(em)}(\theta_1) = \frac{\sigma^2}{M} \frac{\sin^2\theta_3 \cos^2\theta_3}{\left[2(\cos^2\theta_2 + 2\sin^2\theta_4 \sin^2\theta_2)\sin^2\theta_3 \cos^2\theta_3 + (4\cos^2\theta_3 - 1)\sin^2\theta_2 \sin^2\theta_4\right]} \tag{15}$$

$$\mathrm{CRB}^{(em)}(\theta_2) = \frac{\sigma^2}{2M} \tag{16}$$

$$\mathrm{CRB}^{(em)}(\theta_3) = \frac{\sigma^2}{4M} \frac{2(\sin^2\theta_2 + 1)\sin^2\theta_3 \cos^2\theta_3 + (4\cos^2\theta_3 - 1)\sin^2\theta_2 \sin^2\theta_4}{\left[2(\cos^2\theta_2 + 2\sin^2\theta_4 \sin^2\theta_2)\sin^2\theta_3 \cos^2\theta_3 + (4\cos^2\theta_3 - 1)\sin^2\theta_2 \sin^2\theta_4\right]} \tag{17}$$

$$\mathrm{CRB}^{(em)}(\theta_4) = \frac{\sigma^2}{2M} \frac{\cos^2\theta_2 + 8\sin^2\theta_2 \cos^2\theta_3 \sin^2\theta_4}{\left[2(\cos^2\theta_2 + 2\sin^2\theta_4 \sin^2\theta_2)\sin^2\theta_3 \cos^2\theta_3 + (4\cos^2\theta_3 - 1)\sin^2\theta_2 \sin^2\theta_4\right]}. \tag{18}$$

2) Closed-Form CRB for the Dipole Triad:

$$\mathrm{CRB}^{(e)}(\theta_1) = \frac{2\sigma^2}{M} \frac{1}{(\sin^2\theta_4)} \frac{\sin^2\theta_3 \cos^2\theta_3}{\left[(8\cos^2\theta_3 - 1)\sin^2\theta_2 - 4\cos^4\theta_3(2\sin^2\theta_2 - 1 + \cos^2\theta_3 \cos^2\theta_2)\right]} \tag{19}$$

$$\mathrm{CRB}^{(e)}(\theta_2) = \frac{\sigma^2}{2M} \frac{1}{(\sin^2\theta_3 \sin^2\theta_4)} \frac{\left\{\begin{array}{c} -4\cos^6\theta_3 \cos^2\theta_2 + 4\cos^4\theta_3[\cos^2\theta_4 \sin^2\theta_2 + \cos(2\theta)] \\ +8\cos^2\theta_3 \sin^2\theta_2 \sin^2\theta_4 - \sin^2\theta_2 \sin^2\theta_4 \end{array}\right\}}{\left[(8\cos^2\theta_3 - 1)\sin^2\theta_2 - 4\cos^4\theta_3(2\sin^2\theta_2 - 1 + \cos^2\theta_3 \cos^2\theta_2)\right]} \tag{20}$$

$$\mathrm{CRB}^{(e)}(\theta_3) = \frac{\sigma^2}{2M} \frac{1}{(\sin^2\theta_4)} \frac{\left\{\begin{array}{c} 4\cos^6\theta_3 \sin^2\theta_4 \cos^2\theta_2 - 4\cos^4\theta_3[\cos^2\theta_4 \cos^2\theta_2 - \cos(2\theta_2)] \\ +4\cos^2\theta_3 \sin^2\theta_2(1 + \sin^2\theta_4) - \sin^2\theta_2 \sin^2\theta_4 \end{array}\right\}}{\left[(8\cos^2\theta_3 - 1)\sin^2\theta_2 - 4\cos^4\theta_3(2\sin^2\theta_2 - 1 + \cos^2\theta_3 \cos^2\theta_2)\right]} \tag{21}$$

$$\mathrm{CRB}^{(e)}(\theta_4) = \frac{2\sigma^2}{M} \frac{\cos^2\theta_3(4\sin^2\theta_2 + \cos^2\theta_2)}{\left[(8\cos^2\theta_3 - 1)\sin^2\theta_2 - 4\cos^4\theta_3(2\sin^2\theta_2 - 1 + \cos^2\theta_3 \cos^2\theta_2)\right]}. \tag{22}$$

3) Closed-Form CRB for the Loop Triad:

$$\mathrm{CRB}^{(h)}(\theta_1) = \frac{2\sigma^2}{M} \frac{1}{(\sin^2\theta_4)} \frac{\sin^2\theta_3 \cos^2\theta_3}{\left[4\cos^2\theta_3(1 + \sin^2\theta_2) - \sin^2\theta_2 - 4\cos^4\theta_3(1 + \cos^2\theta_2 \sin^2\theta_3)\right]} \tag{23}$$

$$\mathrm{CRB}^{(h)}(\theta_2) = \frac{\sigma^2}{2M} \frac{1}{(\sin^2\theta_4 \cos^2\theta_3)} \frac{\left\{\begin{array}{c} 4\cos^6\theta_3 \cos^2\theta_2 + 4\cos^4\theta_3(\sin^2\theta_2 + \cos^2\theta_4 \sin^2\theta_2 - 2) \\ +4\cos^2\theta_3[1 - \cos(2\theta_4)\sin^2\theta_2] - \sin^2\theta_2 \sin^2\theta_4 \end{array}\right\}}{\left[4\cos^2\theta_3(1 + \sin^2\theta_2) - \sin^2\theta_2 - 4\cos^4\theta_3(1 + \cos^2\theta_2 \sin^2\theta_3)\right]} \tag{24}$$

$$\mathrm{CRB}^{(h)}(\theta_3) = \frac{\sigma^2}{2M} \frac{1}{(\sin^2\theta_4)} \frac{\left\{\begin{array}{c} 4\cos^6\theta_3 \sin^2\theta_4 \cos^2\theta_2 - 4\cos^4\theta_3[1 - \cos^2\theta_2 \cos(2\theta_4)] \\ +4\cos^2\theta_3(1 - \cos^2\theta_4 \cos^2\theta_2 + \sin^2\theta_2 \sin^2\theta_4) - \sin^2\theta_2 \sin^2\theta_4 \end{array}\right\}}{\left[4\cos^2\theta_3(1 + \sin^2\theta_2) - \sin^2\theta_2 - 4\cos^4\theta_3(1 + \cos^2\theta_2 \sin^2\theta_3)\right]} \tag{25}$$

$$\mathrm{CRB}^{(h)}(\theta_4) = \frac{2\sigma^2}{M} \frac{\cos^2\theta_2 + \cos^2\theta_3(4\sin^2\theta_2 - \cos^2\theta_2)}{\left[4\cos^2\theta_3(1 + \sin^2\theta_2) - \sin^2\theta_2 - 4\cos^4\theta_3(1 + \cos^2\theta_2 \sin^2\theta_3)\right]}. \tag{26}$$

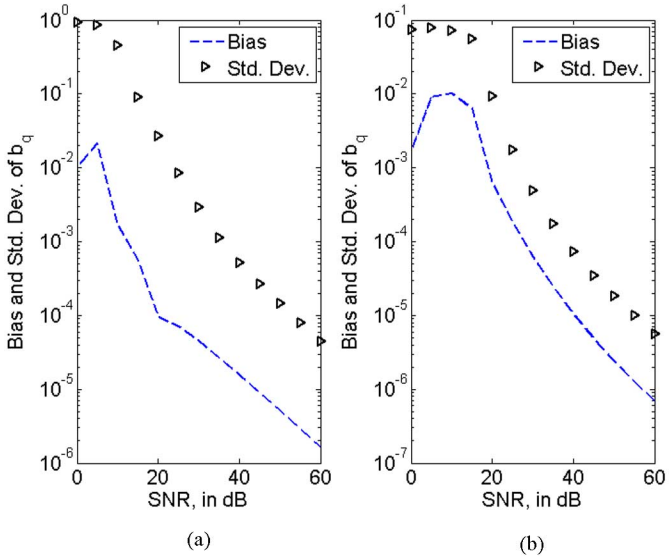


Fig. 2. (a) Estimation bias and standard-deviations of $b_2$ with a second-order PPS versus SNR for the six-component electromagnetic vector-sensor. (b) Estimation bias and standard-deviations of $b_4$ with a fourth-order PPS versus SNR for the six-component electromagnetic vector-sensor.

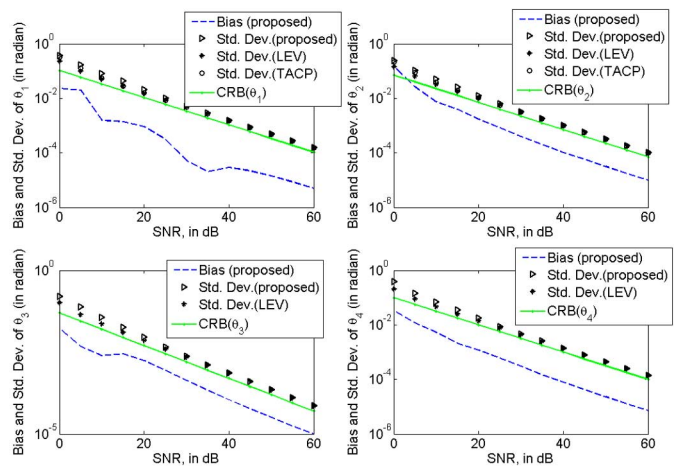


Fig. 3. Estimation bias and standard-deviations of DOA and polarization $\{\theta_1, \theta_2, \theta_3, \theta_4\}$ with a second-order PPS versus SNR for the six-component electromagnetic vector-sensor.

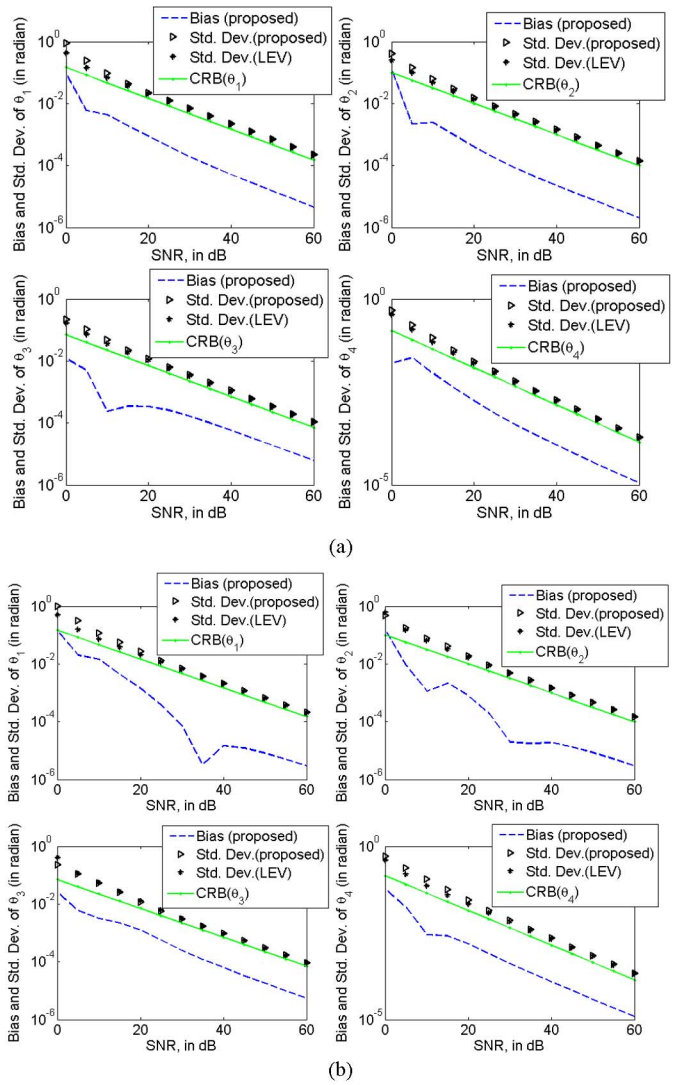


Fig. 4. (a) Estimation bias and standard-deviations of DOA and polarization $\{\theta_1, \theta_2, \theta_3, \theta_4\}$ with a second-order PPS versus SNR for the dipole triad. (b) Estimation bias and standard-deviations of DOA and polarization $\{\theta_1, \theta_2, \theta_3, \theta_4\}$ with a second-order PPS versus SNR for the loop triad.

estimation bias and standard-deviations of DOA and polarization parameters $\{\theta_1, \theta_2, \theta_3, \theta_4\}$ versus SNR $\left(\frac{\mathcal{P}}{\sigma^2}\right)$ for the six-component electromagnetic vector-sensor. The efficiency of the proposed algorithm is compared with the following two algorithms:

a) The Largest EigenVector (LEV) algorithm, which is used to estimate the steering vector of the signal. In this algorithm, the steering vector is estimated from the eigenvector associated with the largest eigenvalue of $\mathbf{R} = \mathbf{X}\mathbf{X}^H$, where $\mathbf{X}$ is defined in (12).

b) The Time Averaging Cross-Product Poynting vector (TACP) algorithm proposed in [13]. From [13], the Poynting vector $\mathbf{u}$ is estimated by

$$\hat{\mathbf{u}} = \frac{\frac{1}{M}\sum_{m=1}^{M} \Re e\left\{\mathbf{x}_e(mT_s) \times \mathbf{x}_h^*(mT_s)\right\}}{\left\|\frac{1}{M}\sum_{m=1}^{M} \Re e\left\{\mathbf{x}_e(mT_s) \times \mathbf{x}_h^*(mT_s)\right\}\right\|}$$

where $\mathbf{x}(mT_s) = \mathbf{a}(\boldsymbol{\theta})s(mT_s) + \boldsymbol{\epsilon}(mT_s)$ as shown in (4), $\mathbf{x}_e(mT_s)$ is the top three rows of $\mathbf{x}(mT_s)$, $\mathbf{x}_h(mT_s)$ is the bottom three rows of $\mathbf{x}(mT_s)$, and $\times$ is the vector-cross operator.

Note that the TACP algorithm proposed in [13] can only be used to estimate the DOA of the incident source and also can only be used for the six-component electromagnetic vector-sensor. But the LEV algorithm can be used to estimate both the DOA and polarization of the source, and it can also be used for the dipole and loop triad. The estimation formulas derived in Section III-E should be adopted when the LEV algorithm is used. It can be observed from Fig. 3 that the proposed algorithm provides a performance comparable with the LEV algorithm, but it can also estimate the polynomial coefficients of the source (see Fig. 2). The TACP algorithm also has a performance similar to the proposed algorithm, but it can not estimate the polarization parameters.

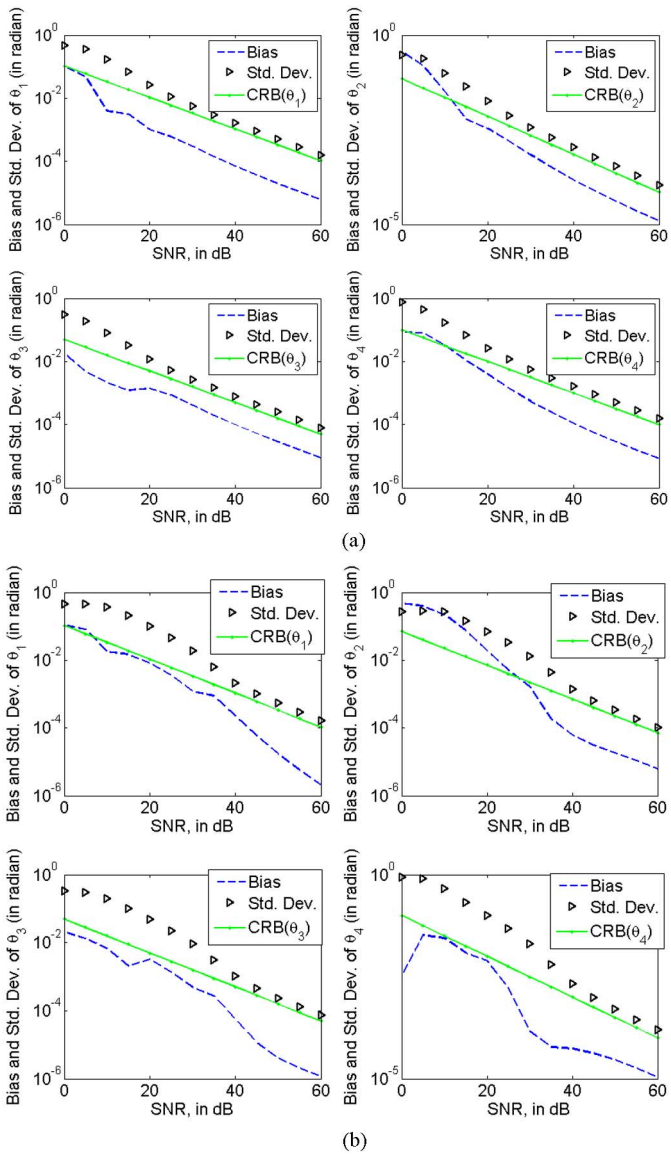


Fig. 5. (a) Estimation bias and standard-deviations of DOA and polarization $\{\theta_1, \theta_2, \theta_3, \theta_4\}$ with a fourth-order PPS versus SNR for the six-component electromagnetic vector-sensor (b) Estimation bias and standard-deviations of DOA and polarization $\{\theta_1, \theta_2, \theta_3, \theta_4\}$ with a seventh-order PPS versus SNR for the six-component electromagnetic vector-sensor.

Fig. 4(a) plots the corresponding bias and standard-deviations for the dipole triad, and Fig. 4(b) plots the corresponding bias and standard-deviations for the loop triad. The standard-deviations of the LEV algorithm are also plotted. Figs. 3 and 4 show that the standard-deviations of all parameters for the six-component electromagnetic vector-sensor are lower than their dipole triad and loop triad counterparts. This is expected as the six-component electromagnetic vector-sensor has more antennas than the triads. It can also be verified by the Cramér–Rao bounds [42].

Fig. 6 compares the DOA estimation of a six-component electromagnetic vector-sensor with an L-shaped array. There are eleven sensors in the L-shaped array and thus in each leg there are six sensors. From the standard-deviations of $\{\theta_1, \theta_2\}$ in Fig. 6, it can be seen that the estimation performance of the six-component electromagnetic vector-sensor is similar to the L-shaped array. However, the L-shaped array has eleven

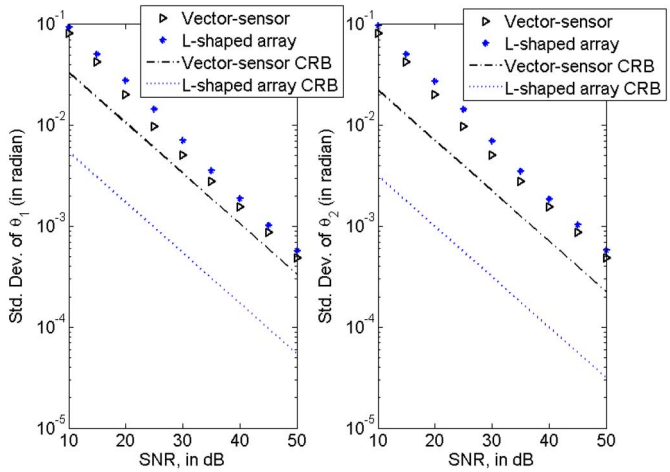


Fig. 6. Estimation standard-deviations of DOA with a second-order PPS versus SNR for the comparison between a six-component electromagnetic vector-sensor and an L-shaped array with six sensors on each leg (in total, eleven sensors are in this L-shaped array). The six sensors on each leg are identically polarized and uniformly spaced at half-wavelength spatial intervals.

sensors and thus needs more computation workload with the proposed algorithm to estimate the DOA of the signal. Fig. 6 also demonstrates that the proposed algorithm can be used in the isotropic sensor array.[5] In this work, we use the polarized vector sensor to estimate not only the DOA of the source, but also the polarization of the signal.

### A. Analysis of the Performance at Low SNR

It is worth pointing out that in Fig. 3, the gap between the estimation standard-deviations of the proposed algorithm and the Cramér–Rao bounds at SNR $\leq$ 10 dB is a little larger than the gap at high SNR. (For the dipole triad and loop triad in Fig. 4(a) and (b), this gap also exists at low SNR.) This is because *multiplicative* noise is introduced when the (5) is used to construct the data-set $\mathbf{x}_{(1)}(t)$. When the SNR is low (SNR $\leq$ 10 dB), the noise affects the algorithm adversely, thus there is a gap between the estimation standard-deviations and the Cramér–Rao bounds. However, when SNR $\geq$ 15 dB, the noise effect decreases, hence the estimation standard-deviations decrease paralleling the Cramér–Rao bounds with the increasing SNR [10]. The standard-deviations are very close to the Cramér–Rao bounds.

In order to further investigate how the *multiplicative* noise affects the proposed algorithm, Fig. 5(a) plots the estimation bias and standard-deviations of $\{\theta_1, \theta_2, \theta_3, \theta_4\}$ with a fourth-order polynomial-phase signal ($\{b_0 = 0.05, b_1 = 0.1, b_2 = 0.13, b_3 = 0.23, b_4 = 0.29\}$), and Fig. 5(b) presents the results with a seventh-order polynomial-phase signal ($\{b_0 = 0.05, b_1 = 0.1, b_2 = 0.13, b_3 = 0.23, b_4 = 0.29, b_5 = 0.31, b_6 = 0.43, b_7 = 0.3\}$) for the six-component electromagnetic vector-sensor. Compare Figs. 3, 5(a), and 5(b), and then locate the SNR value when the estimation standard-deviations begin to decrease paralleling the Cramér–Rao bounds with the increasing SNR. Name this SNR value *the fine SNR point*. For the second-order PPS, *the fine SNR point* is 15 dB. For the

[5]For more comparisons between the polarized vector-sensor and the L-shaped array, please refer to [19].

fourth-order PPS, it is 25 dB and for the seventh-order PPS, it is 40 dB. This is expected as the higher the degree of the PPS, the more multiplicative noise will be introduced in the proposed algorithm. Recall the preprocessing steps in Section III-C to derive the matrix-pencil pair. For the recursive-computation in Section III-C, there will be 1 time multiplication for the second-order PPS, 3 times multiplication for the fourth-order PPS and 6 times multiplication for the seventh-order PPS. In general, there will be $(q-1)$ times multiplication for the $q$-order PPS. Thus, there will be more multiplicative noise introduced for the higher degree PPS. This can also explain why the estimation bias and standard-deviations of $b_q$ decrease slowly at low SNR in Fig. 2. It can be found that if the degree of PPS increases by one, *the fine SNR point* will increase by about 5 dB. However, even for the seventh-order PPS, when SNR $\geq 25$ dB, both the bias and standard-deviations of all the parameters are less than 0.05 radian and so the source can be seen as accurately resolved. Elimination of the multiplicative noise at low SNR will be the subject of further work.

## VI. Conclusion

A new ESPRIT-based algorithm is investigated for azimuth-elevation direction-finding and polarization estimation of one completely-polarized polynomial phase signal with *arbitrary* degree using a single polarized vector-sensor, which can be a six-component electromagnetic vector-sensor, a dipole triad or a loop triad. The matrix-pencil pair used in the ESPRIT algorithm is derived from the temporally displaced data-sets collected by the polarized vector-sensor. The eigenvector of the signal-subspace offers the estimation of the steering vector and closed-form formulas for DOA and polarization parameters for the six-component electromagnetic vector-sensor, the dipole triad and the loop triad are presented. The proposed algorithm requires no *a priori* information of the polynomial-phase signal's coefficients, and no *a priori* knowledge of the polynomial-phase signal's frequency-spectrum. This is the first time that the polarized vector-sensor has been used to resolve the polarization-diversity of the polynomial-phase signal and is thus novel in the literature. However, the degree of the polynomial-phase signal needs to be *a priori* knowledge for the proposed algorithm. How to adopt the proposed algorithm with no *a priori* knowledge of the degree will be addressed in a future study.

The Cramér–Rao bounds of DOA and polarization parameters for the polynomial-phase signal are also derived in this work, explicitly in terms of the signal parameters. The closed-form Cramér–Rao bounds of these parameters are independent of the polynomial coefficients, the degree of the polynomial-phase signal, and also the azimuth-angle of the source.

The proposed algorithm can also be used in the other compositions of polarized vector-sensor, which can yield the closed-form estimation-formulas for DOA and polarization parameters, for example, the other compositions of dipole(s) and/or loop(s) triad, four/five-component electromagnetic vector-sensor. Moreover, this approach can be adapted to the acoustic vector-sensor by utilizing the corresponding mathematical model.

## Appendix
## Closed-Form Cramér–Rao Bounds Derivation From the FIM

With the similar computation in [67], the entities of the FIM in (13) are listed below ($\ell = 0,1,2,\ldots,q;\ \ell_1 = 0,1,2,\ldots,q;\ \ell_2 = 0,1,2,\ldots,q.$):

*FIM of the Dipole Triad:*

$$J^{(e)}_{\theta_1,\theta_1} = \frac{2M(\sin^2\theta_2 + \cos^2\theta_3\cos^2\theta_2)}{\sigma^2};$$
$$J^{(e)}_{\theta_1,\theta_2} = J^{(e)}_{\theta_2,\theta_1} = \frac{2M\sin\theta_3\cos\theta_3\cos\theta_2\cos\theta_4}{\sigma^2};$$
$$J^{(e)}_{\theta_1,\theta_3} = J^{(e)}_{\theta_3,\theta_1} = \frac{-2M\sin\theta_2\cos\theta_4}{\sigma^2};$$
$$J^{(e)}_{\theta_1,\theta_4} = J^{(e)}_{\theta_4,\theta_1} = \frac{M\sin\theta_2\sin(2\theta_3)\sin\theta_4}{\sigma^2};$$
$$J^{(e)}_{\theta_1,b_\ell} = J^{(e)}_{b_\ell,\theta_1} = \frac{2\sin(2\theta_3)\sin\theta_2\sin\theta_4}{\sigma^2}T_s^\ell\sum_{n=1}^{M} n^\ell;$$
$$J^{(e)}_{\theta_2,\theta_2} = \frac{2M\sin^2\theta_3}{\sigma^2};$$
$$J^{(e)}_{\theta_2,\theta_3} = J^{(e)}_{\theta_3,\theta_2} = J^{(e)}_{\theta_2,\theta_4} = J^{(e)}_{\theta_4,\theta_2} = 0;$$
$$J^{(e)}_{\theta_2,b_\ell} = J^{(e)}_{b_\ell,\theta_2} = 0;$$
$$J^{(e)}_{\theta_3,\theta_3} = \frac{2M}{\sigma^2};$$
$$J^{(e)}_{\theta_3,\theta_4} = J^{(e)}_{\theta_4,\theta_3} = 0;$$
$$J^{(e)}_{\theta_3,b_\ell} = J^{(e)}_{b_\ell,\theta_3} = 0;$$
$$J^{(e)}_{\theta_4,\theta_4} = \frac{2M\sin^2\theta_3}{\sigma^2};$$
$$J^{(e)}_{\theta_4,b_\ell} = J^{(e)}_{b_\ell,\theta_4} = \frac{2\sin^2\theta_3}{\sigma^2}T_s^\ell\sum_{n=1}^{M} n^\ell;$$
$$J^{(e)}_{b_{\ell_1},b_{\ell_2}} = J^{(e)}_{b_{\ell_2},b_{\ell_1}} = \frac{2T_s^{(\ell_1+\ell_2)}}{\sigma^2}\sum_{n=1}^{M} n^{(\ell_1+\ell_2)};$$

*FIM of the Loop Triad:*

$$J^{(h)}_{\theta_1,\theta_1} = \frac{2M(\sin^2\theta_3 + \cos^2\theta_3\sin^2\theta_2)}{\sigma^2};$$
$$J^{(h)}_{\theta_1,\theta_2} = J^{(h)}_{\theta_2,\theta_1} = \frac{-2M\sin\theta_3\cos\theta_3\cos\theta_2\cos\theta_4}{\sigma^2};$$
$$J^{(h)}_{\theta_1,\theta_3} = J^{(h)}_{\theta_3,\theta_1} = \frac{-2M\sin\theta_2\cos\theta_4}{\sigma^2};$$
$$J^{(h)}_{\theta_1,\theta_4} = J^{(h)}_{\theta_4,\theta_1} = \frac{M\sin\theta_2\sin(2\theta_3)\sin\theta_4}{\sigma^2};$$
$$J^{(h)}_{\theta_1,b_\ell} = J^{(h)}_{b_\ell,\theta_1} = \frac{2\sin(2\theta_3)\sin\theta_2\sin\theta_4}{\sigma^2}T_s^\ell\sum_{n=1}^{M} n^\ell;$$
$$J^{(h)}_{\theta_2,\theta_2} = \frac{2N\cos^2\theta_3}{\sigma^2};$$
$$J^{(h)}_{\theta_2,\theta_3} = J^{(h)}_{\theta_3,\theta_2} = J^{(h)}_{\theta_2,\theta_4} = J^{(h)}_{\theta_4,\theta_2} = 0;$$
$$J^{(h)}_{\theta_2,b_\ell} = J^{(h)}_{b_\ell,\theta_2} = 0;$$
$$J^{(h)}_{\theta_3,\theta_3} = \frac{2M}{\sigma^2}$$

$$
\begin{bmatrix}
\mathrm{CRB}(\theta_1) & * & * & * \\
* & \mathrm{CRB}(\theta_2) & * & * \\
* & * & \mathrm{CRB}(\theta_3) & * \\
* & * & * & \mathrm{CRB}(\theta_4)
\end{bmatrix}
$$

$$
\begin{aligned}
&= \left[ \begin{bmatrix}
J_{\theta_1,\theta_1} & J_{\theta_1,\theta_2} & J_{\theta_1,\theta_3} & J_{\theta_1,\theta_4} \\
J_{\theta_2,\theta_1} & J_{\theta_2,\theta_2} & 0 & 0 \\
J_{\theta_3,\theta_1} & 0 & J_{\theta_3,\theta_3} & 0 \\
J_{\theta_4,\theta_1} & 0 & 0 & J_{\theta_4,\theta_4}
\end{bmatrix} \right. \\
&\qquad \left. - \begin{bmatrix}
J_{\theta_1,b_0} & \cdots & J_{\theta_1,b_q} \\
0 & \cdots & 0 \\
0 & \cdots & 0 \\
J_{\theta_4,b_0} & \cdots & J_{\theta_4,b_q}
\end{bmatrix} \begin{bmatrix}
J_{b_0,b_0} & \cdots & J_{b_0,b_q} \\
\vdots & \ddots & \vdots \\
J_{b_q,b_0} & \cdots & J_{b_q,b_q}
\end{bmatrix}^{-1} \begin{bmatrix}
J_{b_0,\theta_1} & 0 & 0 & J_{b_0,\theta_4} \\
\vdots & \vdots & \vdots & \vdots \\
J_{b_q,\theta_1} & 0 & 0 & J_{b_q,\theta_4}
\end{bmatrix} \right]^{-1} \\
&= \left[ \begin{bmatrix}
J_{\theta_1,\theta_1} & J_{\theta_1,\theta_2} & J_{\theta_1,\theta_3} & J_{\theta_1,\theta_4} \\
J_{\theta_2,\theta_1} & J_{\theta_2,\theta_2} & 0 & 0 \\
J_{\theta_3,\theta_1} & 0 & J_{\theta_3,\theta_3} & 0 \\
J_{\theta_4,\theta_1} & 0 & 0 & J_{\theta_4,\theta_4}
\end{bmatrix} - \begin{bmatrix}
J_A & 0 & 0 & J_B \\
0 & 0 & 0 & 0 \\
0 & 0 & 0 & 0 \\
J_B & 0 & 0 & J_C
\end{bmatrix} \right]^{-1} \\
&= \begin{bmatrix}
J_{\theta_1,\theta_1} - J_A & J_{\theta_1,\theta_2} & J_{\theta_1,\theta_3} & J_{\theta_1,\theta_4} - J_B \\
J_{\theta_2,\theta_1} & J_{\theta_2,\theta_2} & 0 & 0 \\
J_{\theta_3,\theta_1} & 0 & J_{\theta_3,\theta_3} & 0 \\
J_{\theta_4,\theta_1} - J_B & 0 & 0 & J_{\theta_4,\theta_4} - J_C
\end{bmatrix}^{-1}. \qquad (27)
\end{aligned}
$$

Hence:

$$
\mathrm{CRB}(\theta_1) = \frac{\left(J_C - J_{\theta_4,\theta_4}\right) J_{\theta_3,\theta_3} J_{\theta_2,\theta_2}}{J_{\theta_3,\theta_3} J_{\theta_2,\theta_2} (J_B - J_{\theta_1,\theta_4})^2 + \left(J_{\theta_4,\theta_4} - J_C\right) \left[ J^2_{\theta_1,\theta_3} J_{\theta_2,\theta_2} + J_{\theta_3,\theta_3} \left( J^2_{\theta_1,\theta_2} + J_A J_{\theta_2,\theta_2} - J_{\theta_1,\theta_1} J_{\theta_2,\theta_2} \right) \right]} \qquad (28)
$$

$$
\mathrm{CRB}(\theta_2) = \frac{J_{\theta_3,\theta_3} \left(J_B - J_{\theta_1,\theta_4}\right)^2 + \left(J_{\theta_4,\theta_4} - J_C\right) \left[ J^2_{\theta_1,\theta_3} + \left(J_A - J_{\theta_1,\theta_1}\right) J_{\theta_3,\theta_3} \right]}{J_{\theta_3,\theta_3} J_{\theta_2,\theta_2} (J_B - J_{\theta_1,\theta_4})^2 + \left(J_{\theta_4,\theta_4} - J_C\right) \left[ J^2_{\theta_1,\theta_3} J_{\theta_2,\theta_2} + J_{\theta_3,\theta_3} \left( J^2_{\theta_1,\theta_2} + J_A J_{\theta_2,\theta_2} - J_{\theta_1,\theta_1} J_{\theta_2,\theta_2} \right) \right]} \qquad (29)
$$

$$
\mathrm{CRB}(\theta_3) = \frac{J_{\theta_2,\theta_2} \left(J_B - J_{\theta_1,\theta_4}\right)^2 + \left(J_{\theta_4,\theta_4} - J_C\right) \left[ J^2_{\theta_1,\theta_2} + \left(J_A - J_{\theta_1,\theta_1}\right) J_{\theta_2,\theta_2} \right]}{J_{\theta_3,\theta_3} J_{\theta_2,\theta_2} (J_B - J_{\theta_1,\theta_4})^2 + \left(J_{\theta_4,\theta_4} - J_C\right) \left[ J^2_{\theta_1,\theta_3} J_{\theta_2,\theta_2} + J_{\theta_3,\theta_3} \left( J^2_{\theta_1,\theta_2} + J_A J_{\theta_2,\theta_2} - J_{\theta_1,\theta_1} J_{\theta_2,\theta_2} \right) \right]} \qquad (30)
$$

$$
\mathrm{CRB}(\theta_4) = \frac{J_{\theta_2,\theta_2} J^2_{\theta_1,\theta_3} + J_{\theta_3,\theta_3} \left[ J^2_{\theta_1,\theta_2} + \left(J_A - J_{\theta_1,\theta_1}\right) J_{\theta_2,\theta_2} \right]}{J_{\theta_3,\theta_3} J_{\theta_2,\theta_2} (J_B - J_{\theta_1,\theta_4})^2 + \left(J_{\theta_4,\theta_4} - J_C\right) \left[ J^2_{\theta_1,\theta_3} J_{\theta_2,\theta_2} + J_{\theta_3,\theta_3} \left( J^2_{\theta_1,\theta_2} + J_A J_{\theta_2,\theta_2} - J_{\theta_1,\theta_1} J_{\theta_2,\theta_2} \right) \right]}. \qquad (31)
$$

$$
\begin{aligned}
J^{(h)}_{\theta_3,\theta_4} &= J^{(h)}_{\theta_4,\theta_3} = 0 \\
J^{(h)}_{\theta_3,b_\ell} &= J^{(h)}_{b_\ell,\theta_3} = 0; \\
J^{(h)}_{\theta_4,\theta_4} &= \frac{2M \sin^2\theta_3}{\sigma^2}; \\
J^{(h)}_{\theta_4,b_\ell} &= J^{(h)}_{b_\ell,\theta_4} = \frac{2\sin^2\theta_3}{\sigma^2} T_s^\ell \sum_{n=1}^{M} n^\ell; \\
J^{(h)}_{b_{\ell_1},b_{\ell_2}} &= J^{(h)}_{b_{\ell_2},b_{\ell_1}} = \frac{2T_s^{(\ell_1+\ell_2)}}{\sigma^2} \sum_{n=1}^{M} n^{(\ell_1+\ell_2)}.
\end{aligned}
$$

Note that from [67]: $\mathbf{J}^{(em)} = \mathbf{J}^{(e)} + \mathbf{J}^{(h)}$, where $\mathbf{J}^{(em)}$ denotes the FIM of the six-component electromagnetic vector-sensor, $\mathbf{J}^{(e)}$ refers to the FIM of the dipole triad and $\mathbf{J}^{(h)}$ symbolizes the FIM of the loop triad. Furthermore, all the elements in the FIM are *independent* of the signal's polynomial coefficients $\boldsymbol{\psi} = (b_0, b_1, \ldots, b_q)^T$. Thus, all the following closed-form Cramér–Rao bounds will be independent of polynomial coefficients, as well.

Therefore, for all the three polarized vector-sensors, the FIM can be re-expressed as

$$
\mathbf{J} = \begin{bmatrix}
J_{\theta_1,\theta_1} & J_{\theta_1,\theta_2} & J_{\theta_1,\theta_3} & J_{\theta_1,\theta_4} & J_{\theta_1,b_0} & \cdots & J_{\theta_1,b_q} \\
J_{\theta_2,\theta_1} & J_{\theta_2,\theta_2} & 0 & 0 & 0 & \cdots & 0 \\
J_{\theta_3,\theta_1} & 0 & J_{\theta_3,\theta_3} & 0 & 0 & \cdots & 0 \\
J_{\theta_4,\theta_1} & 0 & 0 & J_{\theta_4,\theta_4} & J_{\theta_4,b_0} & \cdots & J_{\theta_4,b_q} \\
J_{b_0,\theta_1} & 0 & 0 & J_{b_0,\theta_4} & J_{b_0,b_0} & \cdots & J_{b_0,b_q} \\
\vdots & \vdots & \vdots & \vdots & \vdots & \ddots & \vdots \\
J_{b_q,\theta_1} & 0 & 0 & J_{b_q,\theta_4} & J_{b_q,b_0} & \cdots & J_{b_q,b_q}
\end{bmatrix}.
$$

The Cramér–Rao bounds can be computed by (27) and the closed-form results are listed in (28)–(31) at the top of the page.

Symbolic programming by MATLAB of $q \leq 10$ suggests the following[6]:

(a) For the dipole triad and the loop triad:

$$J_A^{(e)} = J_A^{(h)} = \frac{2M \sin^2(2\theta_3) \sin^2\theta_2 \sin^2\theta_4}{\sigma^2},$$
$$J_B^{(e)} = J_B^{(h)} = \frac{4M \sin^3\theta_3 \cos\theta_3 \sin\theta_2 \sin\theta_4}{\sigma^2},$$
$$J_C^{(e)} = J_C^{(h)} = \frac{2M \sin^4\theta_3}{\sigma^2}.$$

(b) For the six-component electromagnetic vector-sensor:

$$J_A^{(em)} = J_A^{(e)} + J_A^{(h)} = \frac{4M \sin^2(2\theta_3) \sin^2\theta_2 \sin^2\theta_4}{\sigma^2},$$
$$J_B^{(em)} = J_B^{(e)} + J_B^{(h)} = \frac{8M \sin^3\theta_3 \cos\theta_3 \sin\theta_2 \sin\theta_4}{\sigma^2},$$
$$J_C^{(em)} = J_C^{(e)} + J_C^{(h)} = \frac{4M \sin^4\theta_3}{\sigma^2}.$$

Then, substitute the entities of the FIM into (28)–(31), the closed-form Cramér–Rao bounds can be obtained as in (15)–(26) in Section IV-B.

## ACKNOWLEDGMENT

The author would like to thank K. Yau for his help in deriving some equations and in checking the correctness of equations in this work. The author would also like to thank the anonymous reviewers for their helpful feedback on a number of key issues in the improvement of the proposed algorithm.

## REFERENCES

[1] A. W. Rihaczek, *Principles of High-Resolution Radar*. New York: McGraw-Hill, 1969.

[2] C. Jordan, *Calculus of Finite Differences*, 3rd ed. New York: AMS Chelsea, 1979.

[3] R. T. Comption, Jr., "The tripole antenna: An adaptive array with full polarization flexibility," *IEEE Trans. Antennas Propag.*, vol. 29, no. 6, pp. 944–952, Nov. 1981.

[4] R. T. Comption, Jr, "The performance of a tripole adaptive array against cross-polarized jamming," *IEEE Trans. Antennas Propag.*, vol. 31, no. 4, pp. 682–685, Jul. 1983.

[5] A. H. Nuttall, "Efficient evaluation of polynomials and exponentials of polynomials for equispaced arguments," *IEEE Trans. Acoust., Speech, Signal Process.*, vol. 35, no. 10, pp. 1486–1487, Oct. 1987.

[6] R. Roy and T. Kailath, "ESPRIT—Estimation of signal parameters via rotational invariance techniques," *IEEE Trans. Acoust., Speech, Signal Process.*, vol. 37, no. 7, pp. 984–995, Jul. 1989.

[7] P. M. Djuric and S. M. Kay, "Parameter estimation of chirp signals," *IEEE Trans. Acoust., Speech, Signal Process.*, vol. 38, no. 12, pp. 2118–2126, Dec. 1990.

[8] S. Peleg and B. Porat, "The Cramer-Rao lower bound for signals with constant amplitude and polynomial phase," *IEEE Trans. Signal Process.*, vol. 39, no. 3, pp. 149–152, Mar. 1991.

[9] S. Peleg and B. Porat, "Estimation and classification of signals with polynomial phase," *IEEE Trans. Inf. Theory*, vol. 37, no. 2, pp. 422–430, Mar. 1991.

[10] B. Ottersten, M. Viberg, and T. Kailath, "Performance analysis of the total least squares ESPRIT algorithm," *IEEE Trans. Signal Process.*, vol. 39, no. 5, pp. 1122–1135, May 1991.

[11] J. Li, "Direction and polarization estimation using arrays with small loops and short dipoles," *IEEE Trans. Antennas Propag.*, vol. 41, no. 3, pp. 379–387, Mar. 1993.

[6]In MATLAB 7.10.0 (R2010a), the function "factorial($n$)" can only be applicable for "$n \leq 21$". If $q = 11$, "factorial(22)" should be used.

[12] S. Peleg, B. Porat, and B. Friedlander, "The achievable accuracy in estimating the instantaneous phase and frequency of a constant amplitude signal," *IEEE Trans. Signal Process.*, vol. 41, no. 6, pp. 2216–2224, Jun. 1993.

[13] A. Nehorai and E. Paldi, "Vector-sensor array processing for electromagnetic source localization," *IEEE Trans. Signal Process.*, vol. 42, no. 2, pp. 376–398, Feb. 1994.

[14] S. Shamsunder, G. B. Giannakis, and B. Friedlander, "Estimating random amplitude polynomial phase signals: A cyclostationary approach," *IEEE Trans. Signal Process.*, vol. 43, no. 2, pp. 492–505, Feb. 1995.

[15] B. Hochwald and A. Nehorai, "Polarimetric modeling and parameter estimation with applications to remote sensing," *IEEE Trans. Signal Process.*, vol. 43, no. 8, pp. 1923–1935, Aug. 1995.

[16] S. Peleg and B. Friedlander, "Multicomponent signal analysis using the polynomial-phase transform," *IEEE Trans. Aerosp. Electron. Syst.*, vol. 32, no. 1, pp. 378–387, Jan. 1996.

[17] S. Barbarossa and V. Petrone, "Analysis of polynomial-phase signals by the integrated generalized ambiguity function," *IEEE Trans. Signal Process.*, vol. 45, no. 2, pp. 316–327, Feb. 1997.

[18] G. T. Zhou and Y. Wang, "Exploring lag diversity in the high-order ambiguity function for polynomial phase signals," *IEEE Signal Process. Lett.*, vol. 4, no. 8, pp. 240–242, Aug. 1997.

[19] K. T. Wong and M. D. Zoltowski, "Uni-vector-sensor ESPRIT for multi-source azimuth, elevation, and polarization estimation," *IEEE Trans. Antennas Propag.*, vol. 45, no. 10, pp. 1467–1474, Oct. 1997.

[20] S. Barbarossa, A. Scaglione, and G. B. Giannakis, "Product high-order ambiguity function for multicomponent polynomial-phase signal modeling," *IEEE Trans. Signal Process.*, vol. 46, no. 3, pp. 691–708, Mar. 1998.

[21] P. J. Kootsookos and J. M. Spanjaard, "An extended Kalman filter for demodulation of polynomial phase signals," *IEEE Signal Process. Lett.*, vol. 5, no. 3, pp. 69–70, Mar. 1998.

[22] S. Golden and B. Friedlander, "A modification of the discrete polynomial transform," *IEEE Trans. Signal Process.*, vol. 46, no. 5, pp. 1452–1455, May 1998.

[23] B. Ristic and B. Boashash, "Comment on the Cramer-Rao lower bound for signals with constant amplitude and polynomial phase," *IEEE Trans. Signal Process.*, vol. 46, no. 6, pp. 1708–1709, Jun. 1998.

[24] A. Scaglione and S. Barbarossa, "On the spectral properties of polynomial-phase signals," *IEEE Signal Process. Lett.*, vol. 5, no. 9, pp. 237–240, Sep. 1998.

[25] S. Golden and B. Friedlander, "Estimation and statistical analysis of exponential polynomial signals," *IEEE Trans. Signal Process.*, vol. 46, no. 11, pp. 3127–3130, Nov. 1998.

[26] M. Z. Ikram, K. Abed-Meraim, and Y. Hua, "Estimating the parameters of chirp signals: An iterative approach," *IEEE Trans. Signal Process.*, vol. 46, no. 12, pp. 3436–3441, Dec. 1998.

[27] P. Tichavsky and P. Handel, "Multicomponent polynomial phase signal analysis using a tracking algorithm," *IEEE Trans. Signal Process.*, vol. 47, no. 5, pp. 1390–1395, May 1999.

[28] S. Valaee, B. Champagne, and P. Kabal, "Localization of wideband signals using least-squares and total least-squares approaches," *IEEE Trans. Signal Process.*, vol. 47, no. 5, pp. 1213–1222, May 1999.

[29] J. M. Francos and B. Friedlander, "Parameter estimation of 2-D random amplitude polynomial-phase signals," *IEEE Trans. Signal Process.*, vol. 47, no. 7, pp. 1795–1810, Jul. 1999.

[30] M. Benidir and A. Ouldali, "Polynomial phase signal analysis based on the polynomial derivatives decompositions," *IEEE Trans. Signal Process.*, vol. 47, no. 7, pp. 1954–1965, Jul. 1999.

[31] B. Barkat and B. Boashash, "Instantaneous frequency estimation of polynomial FM signals using the peak of the PWVD: Statistical performance in the presence of additive Gaussian noise," *IEEE Trans. Signal Process.*, vol. 47, no. 9, pp. 2480–2490, Sep. 1999.

[32] J. A. Legg and D. A. Gray, "Performance bounds for polynomial phase parameter estimation with nonuniform and random sampling schemes," *IEEE Trans. Signal Process.*, vol. 48, no. 2, pp. 331–337, Feb. 2000.

[33] A. M. Zoubir and D. R. Iskander, "Bootstrap modeling of a class of nonstationary signals," *IEEE Trans. Signal Process.*, vol. 48, no. 2, pp. 399–408, Feb. 2000.

[34] K. T. Wong and M. D. Zoltowski, "Closed-form direction-finding with arbitrarily spaced electromagnetic vector-sensors at unknown locations," *IEEE Trans. Antennas Propag.*, vol. 48, no. 5, pp. 671–681, May 2000.

[35] J. Angeby, "Aliasing of polynomial-phase signal parameters," *IEEE Trans. Signal Process.*, vol. 48, no. 5, pp. 1488–1491, May 2000.
[36] A. B. Gershman and M. G. Amin, "Wideband direction-of-arrival estimation of multiple chirp signals using spatial time-frequency distributions," *IEEE Signal Process. Lett.*, vol. 7, no. 6, pp. 152–155, Jun. 2000.
[37] M. D. Zoltowski and K. T. Wong, "Esprit-based 2D direction finding with a sparse array of electromagnetic vector-sensors," *IEEE Trans. Signal Process.*, vol. 48, no. 8, pp. 2195–2204, Aug. 2000.
[38] M. D. Zoltowski and K. T. Wong, "Closed-form eigenstructure-based direction finding using arbitrary but identical subarrays on a sparse uniform rectangular array grid," *IEEE Trans. Signal Process.*, vol. 48, no. 8, pp. 2205–2210, Aug. 2000.
[39] K. T. Wong and M. D. Zoltowski, "Self-initiating music direction finding & polarization estimation in spatio-polarizational beamspace," *IEEE Trans. Antennas Propag.*, vol. 48, no. 8, pp. 1235–1245, Aug. 2000.
[40] K. T. Wong, "Geolocation/beamforming for multiple wideband-FFH with unknown hop-sequences," *IEEE Trans. Aerosp. Electron. Syst.*, vol. 37, no. 1, pp. 65–76, Jan. 2001.
[41] B. Volcker and B. Ottersten, "Chirp parameter estimation from a sample covariance matrix," *IEEE Trans. Signal Process.*, vol. 49, no. 3, pp. 603–612, Mar. 2001.
[42] K. T. Wong, "Direction finding/polarization estimation—Dipole and/or loop Triad(s)," *IEEE Trans. Aerosp. Electron. Syst.*, vol. 37, no. 2, pp. 679–684, Apr. 2001.
[43] A. B. Gershman, M. Pesavento, and M. G. Amin, "Estimating parameters of multiple wideband polynomial-phase sources in sensor arrays," *IEEE Trans. Signal Process.*, vol. 49, no. 12, pp. 2924–2934, Dec. 2001.
[44] H. L. Van Trees, *Detection, Estimation and Modulation Theory, Part IV: Optimum Array Processing*. New York: Wiley, 2002.
[45] M. R. Morelande and A. M. Zoubir, "Model selection of random amplitude polynomial phase signals," *IEEE Trans. Signal Process.*, vol. 50, no. 3, pp. 578–589, Mar. 2002.
[46] M. R. Morelande and A. M. Zoubir, "On the performance of cyclic moments-based parameter estimators of amplitude modulated polynomial phase signals," *IEEE Trans. Signal Process.*, vol. 50, no. 3, pp. 590–616, Mar. 2002.
[47] C. C. Ko, J. Zhang, and A. Nehorai, "Separation and tracking of multiple broadband sources with one electromagnetic vector sensor," *IEEE Trans. Aerosp. Electron. Syst.*, vol. 38, no. 3, pp. 1109–1116, Jul. 2002.
[48] G. M. Phillips, *Interpolation and Approximation by Polynomials*. New York: Springer, 2003.
[49] I. Djurovic and L. Stankovic, "Nonparametric IF and DOA estimation," in *Proc. Int. Symp. Signal Process. Its Appl.*, 2003, vol. 1, pp. 149–152.
[50] D. Rahamim, J. Tabrikian, and R. Shavit, "Source localization using vector sensor array in a multipath environment," *IEEE Trans. Signal Process.*, vol. 52, no. 11, pp. 3096–3103, Nov. 2004.
[51] K. T. Wong, L. Li, and M. D. Zoltowski, "Root-music-based direction-finding & polarization-estimation using diversely-polarized possibly collocated antennas," *IEEE Antennas Wireless Propag. Lett.*, vol. 3, no. 8, pp. 129–132, 2004.
[52] L. Zhang and Y. Peng, "Outlier probability of generalized chirpogram-based estimators for multicomponent polynomial-phase signals," *IEEE Trans. Signal Process.*, vol. 53, no. 2, pp. 576–588, Feb. 2005.
[53] M. Farquharson, P. O'Shea, and G. Ledwich, "A computationally efficient technique for estimating the parameters of polynomial-phase signals from noisy observations," *IEEE Trans. Signal Process.*, vol. 53, no. 8, pp. 3337–3342, Aug. 2005.
[54] S. Miron, N. Le Bihan, and J. I. Mars, "Quaternion-music for vector-sensor array processing," *IEEE Trans. Signal Process.*, vol. 54, no. 4, pp. 1218–1229, Apr. 2006.
[55] N. Ma and J. T. Goh, "Ambiguity-function-based techniques to estimate DOA of broadband chirp signals," *IEEE Trans. Signal Process.*, vol. 54, no. 5, pp. 1826–1839, May 2006.
[56] M. Adjrad and A. Belouchrani, "Estimation of multicomponent polynomial-phase signals impinging on a multisensor array using state space modeling," *IEEE Trans. Signal Process.*, vol. 55, no. 1, pp. 32–45, Jan. 2007.
[57] D. S. Pham and A. M. Zoubir, "Analysis of multicomponent polynomial phase signals," *IEEE Trans. Signal Process.*, vol. 55, no. 1, pp. 56–65, Jan. 2007.
[58] M. Hurtado and A. Nehorai, "Performance analysis of passive low-grazing-angle source localization in maritime environments using vector sensors," *IEEE Trans. Aerosp. Electron. Syst.*, vol. 43, no. 2, pp. 780–789, Apr. 2007.
[59] M. Jabloun, F. Leonard, M. Vieira, and N. Martin, "A new flexible approach to estimate the IA and IF of nonstationary signals of long-time duration," *IEEE Trans. Signal Process.*, vol. 55, no. 7, pp. 3633–3644, Jul. 2007.
[60] N. L. Bihan, S. Miron, and J. Mars, "Music algorithm for vector-sensors array using biquaternions," *IEEE Trans. Signal Process.*, vol. 55, no. 9, pp. 4523–4533, Sep. 2007.
[61] D. S. Pham and A. M. Zoubir, "Estimation of multicomponent polynomial phase signals with missing observations," *IEEE Trans. Signal Process.*, vol. 56, no. 4, pp. 1710–1715, Apr. 2008.
[62] P. Wang, I. Djurovic, and J. Yang, "Generalized high-order phase function for parameter estimation of polynomial phase signal," *IEEE Trans. Signal Process.*, vol. 56, no. 7, pp. 3023–3028, Jul. 2008.
[63] Y. Wu, H. C. So, and H. Liu, "Subspace-based algorithm for parameter estimation of polynomial phase signals," *IEEE Trans. Signal Process.*, vol. 56, no. 10, pp. 4977–4983, Oct. 2008.
[64] Y. Xu, Z. Liu, K. T. Wong, and J. Cao, "Virtual-manifold ambiguity in HOS-based direction-finding with electromagnetic vector-sensors," *IEEE Trans. Aerosp. Electron. Syst.*, vol. 44, no. 4, pp. 1291–1308, Oct. 2008.
[65] Z. Xin, S. Yaowu, G. Hongzhi, and L. Jun, "Parameter estimation of wideband cyclostationary sources based on uni-vector-sensor," in *Proc. Chin. Control Conf.*, 2008, pp. 298–302.
[66] Z. Xin, S. Yaowu, and Y. Wenhong, "2-D DOA and polarization estimation of LFM signals with one electromagnetic vector sensor," in *Proc. Int. Conf. Signal Process.*, 2008, pp. 386–389.
[67] C. K. Au Yeung and K. T. Wong, "CRB: Sinusoid-sources' estimation using collocated dipoles/loops," *IEEE Trans. Aerosp. Electron. Syst.*, vol. 45, no. 1, pp. 94–109, Jan. 2009.
[68] M. Chen and M. Viberg, "Long-range channel prediction based on nonstationary parametric modeling," *IEEE Trans. Signal Process.*, vol. 57, no. 2, pp. 622–634, Feb. 2009.
[69] P. O'Shea and R. A. Wiltshire, "A new class of multilinear functions for polynomial phase signal analysis," *IEEE Trans. Signal Process.*, vol. 57, no. 6, pp. 2096–2109, Jun. 2009.
[70] P. Wang, H. Li, I. Djurovic, and B. Himed, "Instantaneous frequency rate estimation for high-order polynomial-phase signals," *IEEE Signal Process. Lett.*, vol. 16, no. 9, pp. 782–785, Sep. 2009.
[71] R. G. McKilliam and I. V. L. Clarkson, "Identifiability and aliasing in polynomial-phase signals," *IEEE Trans. Signal Process.*, vol. 57, no. 11, pp. 4554–4557, Nov. 2009.
[72] A. Amar, "Efficient estimation of a narrow-band polynomial phase signal impinging on a sensor array," *IEEE Trans. Signal Process.*, vol. 58, no. 2, pp. 923–927, Feb. 2010.
[73] P. Wang, H. Li, I. Djurovic, and B. Himed, "Performance of instantaneous frequency rate estimation using high-order phase function," *IEEE Trans. Signal Process.*, vol. 58, no. 4, pp. 2415–2421, Apr. 2010.
[74] P. O'Shea, "On refining polynomial phase signal parameter estimates," *IEEE Trans. Aerosp. Electron. Syst.*, vol. 46, no. 3, pp. 978–987, Jul. 2010.
[75] A. Amar, A. Leshem, and A. Van der Veen, "A low complexity blind estimator of narrowband polynomial phase signals," *IEEE Trans. Signal Process.*, vol. 58, no. 9, pp. 4674–4683, Sep. 2010.
[76] J. He, S. Jiang, J. Wang, and Z. Liu, "Polarization difference smoothing for direction finding of coherent signals," *IEEE Trans. Aerosp. Electron. Syst.*, vol. 46, no. 1, pp. 469–480, Jan. 2010.
[77] K. T. Wong and X. Yuan, "Vector cross-product direction-finding' with an electromagnetic vector-sensor of six orthogonally oriented but spatially non-collocating dipoles/loops," *IEEE Trans. Signal Process.*, vol. 59, no. 1, pp. 160–171, Jan. 2011.

**Xin Yuan** (S'09) received the B.Eng. degree in electronic information engineering and the M.Eng. degree in information and communication engineering from Xidian University, Xi'an, Shaanxi, China, in 2007 and 2009, respectively.

He is currently working towards a Ph.D. degree at the Hong Kong Polytechnic University. His research interest lies in diversely polarized antenna-array signal processing.